HUBBLE SPACE TELESCOPE AND GROUND-BASED OBSERVATIONS OF SN 1993J AND SN 1998S: CNO PROCESSING IN THE PROGENITORS[1]

Claes Fransson,[2] Peter M. Challis,[3] Roger A. Chevalier,[4] Alexei V. Filippenko,[5] Robert P. Kirshner,[3] Cecilia Kozma,[2] Douglas C. Leonard,[6,7] Thomas Matheson,[3] E. Baron,[8] Peter Garnavich,[9] Saurabh Jha,[5] Bruno Leibundgut,[10] Peter Lundqvist,[2] C. S. J. Pun,[11] Lifan Wang,[12] and J. Craig Wheeler[13]

ABSTRACT

Ground-based and *Hubble Space Telescope* observations are presented for SN 1993J and SN 1998S. SN 1998S shows strong, relatively narrow circumstellar emission lines of N III–V and C III–IV, as well as broad lines from the ejecta. Both the broad ultraviolet and optical lines in SN 1998S indicate an expansion velocity of $\sim$7000 km s^{-1}. The broad emission components of Lyα and Mg II are strongly asymmetrical after day 72 past the explosion and differ in shape from Hα. Different models based on dust extinction from dust in the ejecta or shock region, in combination with Hα from a circumstellar torus, are discussed. It is concluded, however, that the double-peaked line profiles are more likely to arise as a result of optical depth effects in the narrow, cool, dense shell behind the reverse shock than in a torus-like region. The ultraviolet lines of SN 1993J are broad, with a boxlike shape, coming from the ejecta and a cool, dense shell. The shapes of the lines are well fitted by a shell with inner velocity $\sim$7000 km s^{-1} and outer velocity $\sim$10,000 km s^{-1}. For both SN 1993J and SN 1998S a strong nitrogen enrichment is found, with N/C $\approx$ 12.4 in SN 1993J and N/C $\approx$ 6.0 in SN 1998S. From a compilation of all supernovae with determined CNO ratios, we discuss the implications of these observations for the structure of the progenitors of Type II supernovae.

Subject headings: circumstellar matter — nuclear reactions, nucleosynthesis, abundances — stars: evolution — stars: mass loss — supernovae: individual (SN 1993J, SN 1998S)

1. INTRODUCTION

The nature of the progenitors of the different types of supernovae (SNe) is still debated. One of the main unknowns is the amount of mass loss suffered by the progenitor before the explosion. The extent of the mass loss, driven either by stellar winds in single stars or by binary evolution, causes widely different progenitor structures. Because the supernova light curve and spectrum to a large extent are functions of the mass of the hydrogen and helium envelope, the mass-loss history is a key ingredient in understanding the various observational signatures, manifested in the many separate classes of core-collapse SNe. Mass loss affects the chemical composition of the ejecta; hence, detailed spectral studies of the different types of SNe and their environments can shed some light on this issue.

A large number of SNe have now shown various types and degrees of circumstellar interaction; see Filippenko (1997) for a recent review. Both of the "Type II linear supernovae" (SNe II-L) 1979C and 1980K showed evidence for circumstellar interaction in their radio emission (Weiler et al. 1986), as well as in the ultraviolet (UV) emission in the case of SN 1979C (Panagia et al. 1980; Fesen et al. 1999). The circumstellar medium most likely originates from the dense, slow superwind of the red supergiant progenitor. Type Ib and Ic SNe are believed to have lost most of their hydrogen envelope prior to exploding. They in general show both radio emission and X-ray emission caused by circumstellar interaction. Because of the high wind speed ($\gtrsim$1000 km s^{-1}) of the Wolf-Rayet progenitor, the wind in this case is considerably less dense compared to that of SNe II-L and II-P.

SN 1993J provided a link between SNe II and SNe Ib in that it underwent a transition from a Type II spectrum at early epochs to a Type Ib-like spectrum at $\sim$300 days (Filippenko et al. 1993, 1994; Finn et al. 1995; Barbon et al. 1995); see Filippenko & Matheson (2004) for a recent review. At early epochs it already showed the typical signatures of circumstellar interaction at radio (Van Dyk et al. 1994), UV (Fransson & Sonneborn 1994), and X-ray (Zimmermann et al. 1994) wavelengths. After about 1 year, the optical spectrum became dominated by emission lines excited by the circumstellar interaction (Filippenko et al. 1994; Patat et al. 1995; Matheson et al. 2000a, 2000b).

Type IIn supernovae (e.g., Filippenko 1997) have optical spectral signatures of a circumstellar medium (CSM) present already at early phases. Although they show considerable variation from object to object, the common characteristics are strong, relatively narrow emission lines after a few weeks, or perhaps earlier; these lines are thought to be produced by the interaction

[2] Department of Astronomy, Stockholm University, AlbaNova, SE-106 91 Stockholm, Sweden; claes@astro.su.se email.

[3] Harvard-Smithsonian Center for Astrophysics, 60 Garden Street, Cambridge, MA 02138.

[4] Department of Astronomy, University of Virginia, P.O. Box 3818, Charlottesville, VA 22903.

[5] Department of Astronomy, University of California, Berkeley, CA 94720-3411.

[6] Five College Astronomy Department, University of Massachusetts, Amherst, MA 01003-9305.

[7] Department of Astronomy, 105-24 Caltech, Pasadena, CA 91125.

[8] Department of Physics and Astronomy, University of Oklahoma, 440 West Brooks, Norman, OK 73019-0261.

[9] Department of Physics, University of Notre Dame, 225 Nieuwland Science Hall, Notre Dame, IN 45656.

[10] European Southern Observatory, Karl-Schwarzschild-Strasse 2, D-85748 Garching, Germany.

[11] Department of Physics, University of Hong Kong, Pokfulam Road, Hong Kong.

[12] Institute for Nuclear and Particle Astrophysics, E. O. Lawrence Berkeley National Laboratory, Berkeley, CA 94720.

[13] Department of Astronomy, University of Texas, Austin, TX 78712.

TABLE 1
Log of *HST* FOS and STIS Observations of SN 1993J

UT Date	Epoch[a] (days)	Grating[b]	Dispersion (Å pixel^{-1})	Exposure (s)	Range (Å)
1995 Jan 26.............	670	G270H	2.05	3600	2221–3301
		G400H	3.00	2600	3240–4822
1996 Feb 23............	1063	G160L	6.64	8200	1140–2508
		G270H	2.05	4800	2221–3301
1997 Jan 24.............	1399	G160L	6.64	22200	1140–2508
		G270H	2.05	6400	2221–3301
1998 Feb 21............	1792	G230L	1.58	9300	1568–3184
1998 Apr 17............	1847	G140L	0.60	20200	1140–1730
2000 Apr 18............	2579	G140L	0.60	19500	1140–1730
2000 Apr 24............	2585	G230L	1.58	3000	1570–3180

[a] Based on an assumed explosion date of 1993 March 27.5 UT.
[b] FOS, 1995–1997; STIS, 1998–2000.

between the supernova ejecta and the CSM. In extreme cases (e.g., SN 1988Z: Turatto et al. 1993; Chugai & Danziger 1994) the CSM is clearly very dense and extensive, and the interaction lasts for many years. Occasionally (e.g., SN 1994W; Chugai et al. 2004) there is evidence that much of the CSM was produced just a short time before the explosion. In addition, the light curves of SNe IIn have a large variation in terms of the relative importance of the radioactive heating and energy input from circumstellar interaction. However, the nature and relation of the SNe IIn to other SN types are not clear (for a discussion, see Nomoto et al. 1995). SN 1998S represents one of the best-studied examples of this type of supernova.

In contrast to SN 1993J, the optical spectrum of SN 1998S was dominated by circumstellar interaction even at early epochs. Bowen et al. (2000) found that many low-ionization UV lines had a narrow P Cygni component, which they interpret as a wind with velocity ∼50 km s^{-1}, as well as a more highly ionized component with velocity ∼300 km s^{-1}. This was later confirmed from ground-based observations by Fassia et al. (2001). Chugai (2001) argued that the narrow core and smooth high-velocity wings of the Hα line at early epochs could be understood as a result of electron scattering in a dense circumstellar shell extending from the supernova. While the observations during the first months showed fairly symmetrical line profiles, the lines changed character after ∼100 days: Hα, as well as He I λ10830, displayed a highly asymmetrical triple-peaked structure (Gerardy et al. 2000). Infrared observations showed evidence for CO formation at ∼95 days and dust formation at ∼225 days (Fassia et al. 2000; Gerardy et al. 2002). The supernova also showed strong X-ray emission at late epochs (Pooley et al. 2002). No radio emission was seen at early epochs. However, by 310 days emission was detected at 8.46 GHz, and subsequently also at 1.47 and 4.89 GHz (Pooley et al. 2002). The late turn-on and its frequency dependence may be understood as a result of strong free-free absorption by the circumstellar gas.

One of the most important indicators of the extent of mass loss is the relative abundances of the CNO elements. Depending on the mass lost and the degree of mixing, CNO burning products may be seen in either the CSM or in the outer parts of the progenitor, and therefore in the supernova (e.g., Meynet & Maeder 2000; Heger & Langer 2000; Wellstein & Langer 1999). Evidence for such CNO processing has been seen in SN 1979C (Fransson et al. 1984), SN 1987A (Fransson et al. 1989), and SN 1995N (Fransson et al. 2002). In this paper we add two more cases.

SN 1993J and the Type IIn SN 1998S are among the best-observed circumstellar interactors to date. In this paper we report on UV observations of these two SNe and on their implications for the abundances of the CNO elements. Early-epoch *Hubble Space Telescope* (*HST*) observations of both SNe have previously been discussed, but mainly in the context of the outer regions of the supernova ejecta (Jeffery et al. 1994; Houck & Fransson 1996; Lentz et al. 2001). In this paper we concentrate on the late-epoch observations, where most of the indicators of circumstellar interaction are present. In addition to the *HST* observations, we also add new ground-based observations. Based on the complete evolution of the line profiles, we discuss implications of the shapes of these for the physics of the interaction region. The analysis in this phase is simplified by the basically nebular conditions of the line-emitting gas.

SN 1993J was discovered on 1993 March 28.9 (Ripero et al. 1993), while SN 1998S was discovered on 1998 March 2.68 UT (Li et al. 1998; Qiu et al. 1998). Here we adopt explosion dates of 1993 March 27.5 for SN 1993J (Lewis et al. 1994) and 1998 March 2 for SN 1998S. The true explosion date of SN 1998S was probably somewhat earlier, of course, but by a negligible amount given the late-time phases studied here. Richmond et al. (1994) discuss the reddening of SN 1993J and argue for a most likely value of $E_{B-V} = 0.2$ mag, which we adopt. For SN 1998S Leonard et al. (2000) find a reddening of $E_{B-V} = 0.23$ mag. The distance to SN 1993J is 3.63 Mpc (Freedman et al. 1994), and the recession velocity is -135 km s^{-1} (Vladilo et al. 1994). The recession velocity of SN 1998S is 846.9 km s^{-1} (Fassia et al. 2001), and we adopt a distance of 17 Mpc (Tully 1988).

2. OBSERVATIONS

The *HST* observations in this paper were obtained with the Faint Object Spectrograph (FOS) and the Space Telescope Imaging Spectrograph (STIS). Tables 1 and 2 give the journal of observations of SN 1993J and SN 1998S, including exposure times, gratings used, their dispersion, and the wavelength ranges covered. The FOS spectra were obtained with the G160L, G270H, and G400H gratings, while the STIS spectra were obtained with gratings G140L, G230L, and G430L. All spectra were calibrated by the FOS and STIS pipelines at the Space Telescope Science Institute. The Lyα region in the FOS spectra of SN 1993J on days 1063 and 1399 is dominated by the geocoronal Lyα, so it is not used in this paper. In the STIS spectra on days 1792–2585 this component could be subtracted successfully.

To complement the *HST* observations, optical low-dispersion spectra of SN 1998S for days 29, 75, 257–258, 431, and 440

TABLE 2
Log of *HST* STIS Observations of SN 1998S

UT Date	Epoch[a] (days)	Grating	Dispersion (Å pixel^{-1})	Exposure (s)	Range (Å)
1998 Mar 16	14	G140L	0.60	2160	1140–1730
		G230L	1.58	3920	1570–3180
		G430L	2.73	180	2900–5700
1998 Mar 30	28	G140L	0.60	6860	1140–1730
		G230L	1.58	2400	1570–3180
		G430L	2.73	300	2900–5700
1998 May 13...........	72	G140L	2.05	6860	1140–1730
		G230L	2.05	5200	1570–3180
		G430L	3.00	300	2900–5700
1998 Oct 26	238	G140L	2.05	6730	1140–1730
		G230L	2.05	5000	1570–3180
		G430L	3.00	700	3240–4822
1999 Jun 30	485	G140L	2.05	5500	1140–1730
		G230L	2.05	11600	1570–3180

[a] From the date of discovery on 1998 March 2 UT (see text).

were obtained with the FAST spectrograph (Fabricant et al. 1998) on the 1.5 m Tillinghast telescope at the Fred L. Whipple Observatory (FLWO). The FAST spectrograph employs a 2688×512 pixel Loral CCD with a spatial scale of $1\farcs1$ pixel^{-1} in the binning mode used for these observations. Details of the exposures are given in Table 3. The data were reduced in the standard manner with IRAF[14] and our own routines. Wave-

[14] IRAF is distributed by the National Optical Astronomy Observatory, which is operated by the Association of Universities for Research in Astronomy, Inc., under cooperative agreement with the National Science Foundation.

length calibration was accomplished with He-Ne-Ar lamps taken immediately after each supernova exposure. Small-scale wavelength adjustments derived from night-sky lines in the supernova frames were also applied. Spectrophotometric standards used in the reductions are listed in Table 3. We attempted to remove telluric lines using the well-exposed continua of the spectrophotometric standards (Matheson et al. 2000a). The FLWO spectra were observed, in general, within $\sim 10°$ of the parallactic angle to minimize losses from atmospheric dispersion (Filippenko 1982).

To complete the temporal coverage of the optical spectra of SN 1998S we have also included spectra up to day 494 from the

TABLE 3
Log of Ground-based Observations of SN 1998S

UT Date	Epoch[a] (day)	Instrument	Range (Å)	Resolution (Å)	P.A. (deg)	Parallactic Angle (deg)	Air Mass	Standard Star	Seeing (arcsec)	Slit (arcsec)	Exposure (s)
1998 Mar 31	29	FLWO	3720–7521	7.0	90	65	1.12	Feige 34	2–3	3	3 × 300
1998 May 16....	75	FLWO	3720–7540	7.0	90	177	1.04	Feige 34	1–2	3	660
1998 Jun 18	108	Lick	3300–5400	8	66	69	1.83	Feige 34	1.5	2	2 × 300
1998 Jun 18	108	Lick	5100–10400	12	66	69	1.83	HD 84937	1.5	2	2 × 300
1998 Jul 17	137	Lick	3300–5400	8	71	71	1.74	BD +28°4211	2.0	2	900
1998 Jul 17	137	Lick	5200–10400	12	71	71	1.74	BD +26°2606	2.0	2	900
1998 Jul 23	143	Lick	4300–7050	10	73	72	1.68	BD +26°2606	1.5	2	900
1998 Jul 23	143	Lick	3280–5420	6	73	72	1.78	BD +28°4211	1.5	2	720
1998 Jul 23	143	Lick	6050–8050	7	73	72	1.78	BD +26°2606	1.5	2	720
1998 Nov 14....	257	FLWO	3720–7521	7.0	90	81	1.19	Feige 34	3	3	2 × 1200
1998 Nov 15....	258	FLWO	3720–7521	7.0	90	83	1.22	Feige 34	2–3	3	3 × 1200
1998 Nov 25....	268	Lick	5200–10200	12	88	87	1.25	BD +17°4708	2.2	2	1272+2000
1999 Jan 6........	310	Keck 2	4360–6860	6	175	184	1.13	HD 19445	1.2		450
1999 Jan 10......	314	Lick	3350–5500	8	180	38	1.02	BD +28°4211	1.5	2	2 × 1800
1999 Jan 10......	314	Lick	5200–10500	12	180	38	1.02	BD +74°408	1.5	2	2 × 1800
1999 Mar 12	375	Lick	3276–5400	8	185	115	1.06	Feige 34	1.8	2	1800
1999 Mar 12	375	Lick	5250–10500	12	185	115	1.06	HD 19445	1.8	2	1800
1999 May 7......	431	FLWO	3720–7521	7.0	0	175	1.04	Feige 66	1–2	3	3 × 1200
1999 May 16....	440	FLWO	3720–7540	7.0	90	127	1.12	Feige 34	1–2	3	4 × 1200
1999 Jul 9	494	Lick	3290–5400	8	70	71	1.7	Feige 34	2.3	3	2 × 1500
1999 Jul 9	494	Lick	5156–10550	12	70	71	1.7	BD +26°2606	2.3	3	2 × 1500
1999 Dec 5	643	Keck 2	4000–10000	15	50	51	1.2	HD 84937	1.8	1.0	900
1999 Dec 15	653	Keck 2	5644–6935	2.5	65	65	1.37	HD 84937	1	1.0	300 + 600
2004 Jan 18......	2148	MMT	3270–8460	8.0	130	122	1.07	Feige 34/HD 84937	1.5	2	2 × 1800

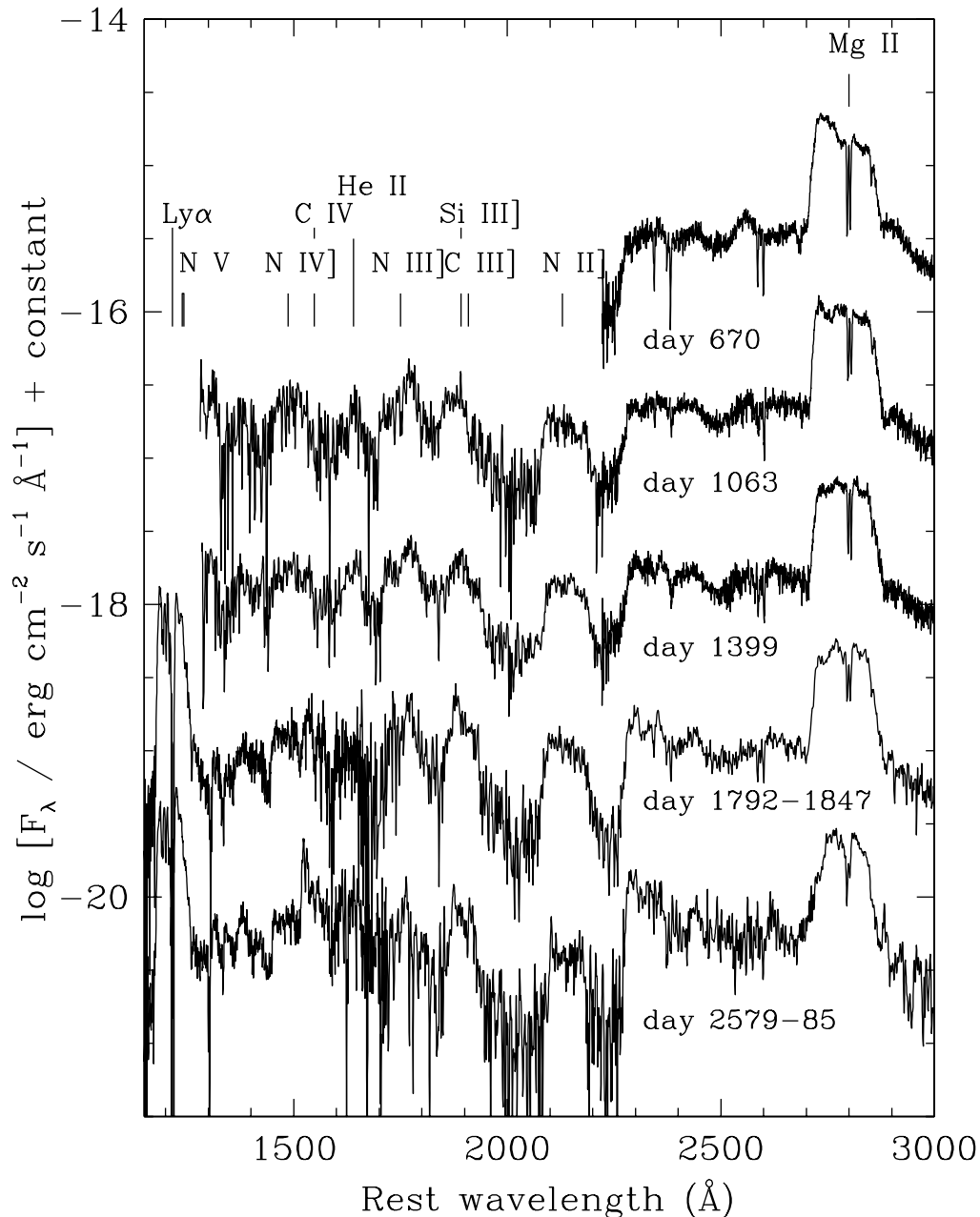[a] From the date of discovery on 1998 March 2 UT (see text).

Fig. 1.—Late-time evolution of the spectrum of SN 1993J, with epochs (days after the explosion) indicated. Each spectrum is shifted down by 1.0 dex with respect to the previous one. The Lyα line in the spectra at days 1063 and 1399 is severely affected by geocoronal Lyα and has therefore been omitted.

Lick Observatory, published by Leonard et al. (2000); see our Table 3. In addition to these, two spectra on days 643 and 653 were also obtained at the Keck II 10 m telescope with LRIS (Oke et al. 1995), and one very late time spectrum (day 2148) was obtained with the MMT 6.5 m telescope using the Blue Channel spectrograph (Schmidt et al. 1989). All data were reduced in a manner similar to that described above for the FLWO spectra. For the spectra on days 643 and 2148 the conditions were such that a proper background subtraction was difficult. These spectra may therefore be contaminated by the galaxy background, and the fluxes may be correspondingly uncertain. Note that our spectrum from day 653 is also shown in the Hα compilation in Pozzo et al. (2004).

Details of the Keck observations of SN 1993J on days 670, 976, 1766, and 2454, included in this paper, are given by Matheson et al. (2000a). In addition, we have included one

spectrum of SN 1993J taken with MMT on 1997 April 8 (day 1473).

3. RESULTS

3.1. *SN 1993J*

HST observations of SN 1993J at early phases were discussed in Jeffery et al. (1994) and Baron et al. (1994). In this paper we limit ourselves to the nebular phase, when the spectrum is dominated by the circumstellar interaction and the line profiles are easier to identify and analyze.

Figure 1 shows the *HST* spectra of SN 1993J from 1995 January to 2000 April (days 670–2585), where we have noted the positions of some of the strongest spectral features. As discussed below, however, some of these are likely to be blends of several lines. Note that the overlap region of the short-wavelength and
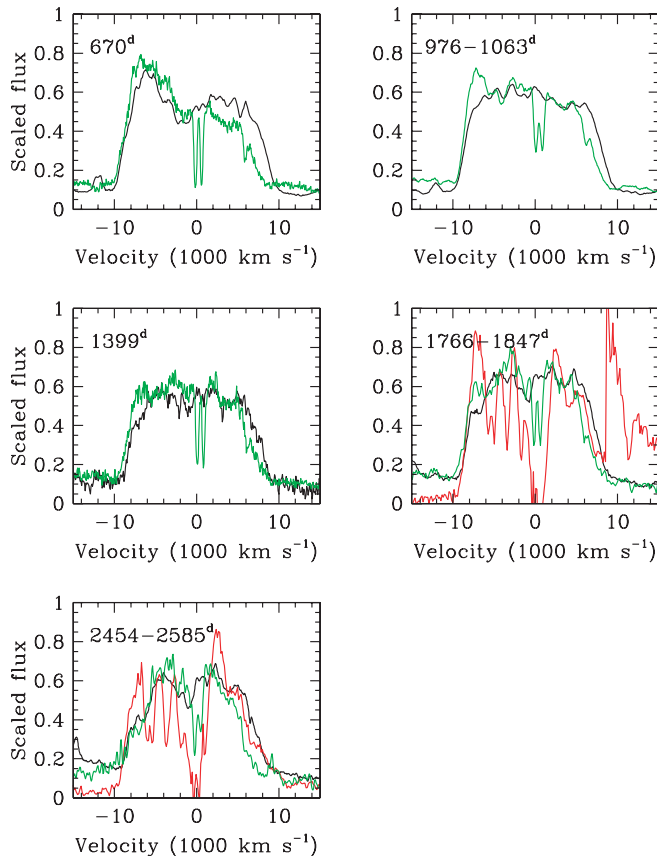
Fig. 2.—Evolution of the line profiles of Hα (*black*), Lyα (*red*), and Mg II (*green*) in SN 1993J. The flux scale differs among the lines. The epoch (days after the explosion) is given in each panel. In the *HST* spectra from days 1063 and 1399 the Lyα line is severely contaminated by geocoronal Lyα and is therefore not shown. There was no observation of Lyα on day 670.

Fig. 3.—Observed line profiles of Hα, [N II], and Mg II in SN 1993J. For [N II] and Mg II we have averaged the day 1063 and 1399 spectra, while Hα is from the day 976 Keck spectrum. The flux scale differs among the lines. The thick line gives the expected line profile for a shell of constant emissivity, inner velocity $V_{in} = 7000$ km s^{-1}, and outer velocity $V_{out} = 10,000$ km s^{-1}.

long-wavelength UV detectors in the range 1600–1700 Å is affected by an increased noise level.

During this whole time in the nebular phase, the spectrum is remarkably constant. The far-UV region is dominated by the strong Lyα emission line, probably blended with N V λλ1238.8, 1242.8. The region shortward of ∼2000 Å forms a pseudo-continuum of blended lines of highly ionized nitrogen, carbon, and oxygen, which we discuss in more detail below. The well-defined line at ∼2140 Å is most likely due to N II] λλ2139.7, 2143.5. The presence of this prominent line indicates a strong nitrogen enrichment, as we confirm later. The plateau longward of ∼2280 Å is probably formed mainly of Fe II resonance lines, although a blend of C II] 2323.5–2328.1, O III] 2320.9–2331.4, and Si II] λ2334.6 is likely to explain the feature at ∼2332 Å. Finally, the near-UV region is dominated by the prominent Mg II λλ2795.5, 2802.7 doublet.

The most interesting temporal change is in the shape of the Mg II line. This evolution is similar to that seen in Hα (Matheson et al. 2000a). In Figure 2 we compare the Lyα, Hα, and Mg II line profiles. The Hα profiles are taken from Matheson et al. (2000a). From the figure we see that the shapes of both the Hα and Mg II lines change in concordance with each other. On day 670 both lines are clearly asymmetrical, with the blue side of Mg II a factor of ∼2.2 stronger than the red. The asymmetry of Hα is considerably smaller, with a blue-to-red intensity ratio of ∼1.1. By day 1063 this asymmetry has decreased for both lines, and for the later epochs the two sides have nearly equal strength. The Lyα line is strongly affected by geocoronal
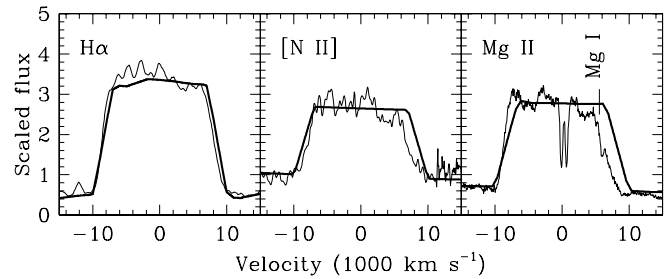
emission, which makes a comparison with the other lines uncertain.

As has been previously noted (e.g., Filippenko et al. 1994; Finn et al. 1995; Patat et al. 1995; Matheson et al. 2000b), the line profiles after ∼1 year, in particular that of Hα, can best be described as boxlike. This strongly indicates that the emission comes from a relatively thin shell in the expanding gas. Matheson et al. (2000b) found during this period a maximum velocity of ∼9000–10,600 km s^{-1} for the blue edge of the Hα line, and a slightly lower velocity for the red edge.

Of the UV lines, only the Mg II and [N II] λλ2139.7, 2143.5 lines are unblended and have sufficiently high signal-to-noise ratio (S/N) to warrant a detailed line fit. As is seen from Figure 1, the UV spectrum does not change appreciably from 1996 January to 1997 February. To increase the S/N, we therefore average the day 1063 and day 1399 spectra. We then fit these line profiles, as well as the Hα profile from the Keck spectrum on day 976, with a shell having inner velocity V_{in} and outer velocity V_{out}; see Fransson (1984a) for details. The variation of the emissivity within the shell is of minor importance; as long as the shell is reasonably thin, it only affects the wings of the lines (for $V > V_{in}$).

In Figure 3 we show a fit for the three lines with $V_{in} = 7000$ and $V_{out} = 10,000$ km s^{-1}. Given the simplicity of the model, the fits are surprisingly good, especially that of Hα. There is a minor asymmetry in the Hα line, where the red side would be better fitted, with $V_{in} = 6000$ and $V_{out} = 10,000$ km s^{-1}. There is some indication that the [N II] line has a somewhat smaller width than Hα, with $V_{in} \approx 6000$ km s^{-1}. Because of the lower S/N compared to Hα, however, this is hardly significant.

Part of the deficit on the red side of Mg II is caused by the interstellar Mg I λ2852 absorption line from the host galaxy of SN 1993J (M81) and the Milky Way (see de Boer et al. 1993). This is, however, unlikely to explain the entire asymmetry. Additional interstellar Fe II absorption lines may possibly contribute, but these should not be stronger than the Mg I absorption, and therefore they only marginally affect the line. It is also difficult to understand the red deficit as a result of an intrinsic asymmetry of the Mg II-emitting region, since this should coincide with the Hα line, which does not show such a pronounced effect. In § 4.2 we discuss a different explanation based on optical depth effects in the emitting region.

Of the other UV lines, only N IV] λ1486 is isolated enough for blending not to be important. The noise, however, makes the profile of this line uncertain. With this caveat, the line can be fitted with the same line profile as for Hα.

For the region below 2000 Å, which is of most interest for the CNO abundance analysis, the blending of the lines requires a detailed spectral synthesis to derive accurate line fluxes. Be-
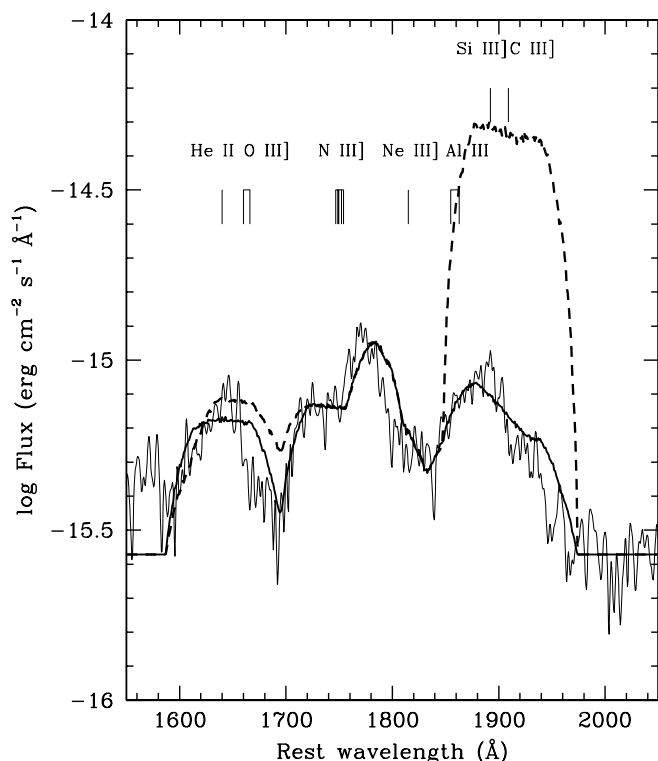
FIG. 4.—Spectral synthesis model of the O III], N III], and C III] regions of SN 1993J. The observed spectrum shown is the average of the day 1063 (1996 February 23) and day 1399 (1997 January 24) spectra. The solid synthetic spectrum has N/C = 12.4 and N/O = 6, while the dashed line shows the expected spectrum for solar CNO ratios, N/C = 0.25 and N/O = 0.12.

Line	Relative Flux[a]
He II 1640.4	0.50
O III] 1660.8, 1666.1..............	0.13
N III] 1746.8–1753.4	1.00
Ne III] 1814.6	1.00
Si III] 1882.7, 1892.0	0.12
C III] 1906.7, 1909.6..............	0.63

[a] Fluxes relative to N III].

$\lambda1814.6$ by Al III $\lambda\lambda1854.7$, 1862.8. The scattered Ne III] flux gives rise to some of the emission at ~1880 Å. The uncertainties in the fluxes of the individual lines are difficult to quantify, but we estimate the N III] and C III] fluxes to be accurate to $\pm30\%$.

Finally, we comment on the N IV] $\lambda1486$ and C IV $\lambda\lambda1548.9$, 1550.8 lines (see Fig. 1). While the N IV] line is clearly seen, the C IV doublet is unfortunately swamped by the continuum, as well as affected by the interstellar absorption. We can therefore only give a lower limit to the (N IV] $\lambda1486$)/(C IV $\lambda\lambda1548.9$, 1550.8) ratio of ~1.5. This limit is conservative, because we have assumed a lower continuum for C IV than for N IV]; it is likely that the true ratio is considerably higher.

3.2. SN 1998S

In Figure 5 we show the full spectral evolution of SN 1998S for the epochs where *HST* observations exist, while in Figure 6 the important far-UV region is shown in more detail. Finally, we show in Figure 7 the spectral evolution in the optical range for the nebular phase. This complements the observations in Leonard et al. (2000) by adding the very late spectra at 643 and 2148 days.

The spectrum during the first 1–2 months is mainly a continuum with superposed P Cygni lines, as discussed by Lentz et al. (2001). By day 72 several strong emission lines have emerged. The lines can be divided into narrow lines with FWHM $\lesssim300$ km s^{-1} and broad lines extending up to $\sim10,000$ km s^{-1} (half-width near zero intensity; HWZI); they are likely to originate in the CSM and in ejecta gas.

3.2.1. Broad Lines

The strongest of the broad lines are Lyα, Hα, and Mg II $\lambda\lambda2795.5$, 2802.7. In Figure 8 we compare their profiles throughout the course of the *HST* observations. The flux scale is linear and varies for the different lines and dates to facilitate a comparison. During the first two epochs only the central absorptions of Lyα and Mg II are visible. These features are shown in detail in high-resolution spectra published by Bowen et al. (2000), where both a Galactic and a host galaxy component are seen, in addition to a ~350 km s^{-1} component from the CSM of SN 1998S. Lyα is even more affected by interstellar absorptions. Because of the large H I column density, these lines show strong damping wings, extending ~10 Å from the line center.

On day 72 and later, both Lyα and Mg II have developed a strong blue emission component. The shapes of the Lyα and Mg II lines are similar within the uncertainties, with the blue wing at least a factor of 10 stronger than the red. The lines extend on day 72 to ~8000 km s^{-1} (HWZI). In the later spectra a marginal decrease in this velocity can be seen.

cause of the higher S/N of the N III]–C III] region compared to the N IV]–C IV region, we concentrate on the former. Based on line identifications in UV spectra of other supernovae and other photoionization-dominated objects, we have added lines from all ions in the interval 1600–2000 Å at the appropriate wavelengths and adjusted the relative fluxes to provide a best fit. The lines included are He II $\lambda1640.4$, O III] $\lambda\lambda1660.8$, 1666.2, N III] $\lambda\lambda1746.8$–1754.0, Ne III] $\lambda1814.6$, Si III] $\lambda\lambda1882.7$, 1892.0, and C III] $\lambda\lambda1908.7$. The relative intensities of the individual multiplet components are calculated for $T_e = 15,000$ K and $n_e = 10^8$ cm^{-3}, values typical of the conditions in the outer ejecta. From models of the ejecta one also expects Al III to have a substantial fractional abundance. Because Al III $\lambda\lambda1854.7$, 1862.8 are resonance lines, they in general have high optical depths, causing a scattering of lines blueward of Al III (especially the N III and Ne III] lines) to longer wavelengths. We calculated this scattering by a Monte Carlo procedure, taking the doublet nature of the lines into account. For all lines we assume a boxy line profile determined from N II] $\lambda\lambda2139.68$, 2143.5 (see above). The Al III scattering is assumed to take place in the same region.

To increase the S/N in the abundance analysis we again use the averaged day 1063 and day 1399 spectrum. The result of the best-fit model is shown in Figure 4, and the individual line fluxes relative to the total flux of the N III] multiplet are given in Table 4. Because of blending and resonance scattering, the resulting spectrum has a complicated form. We note that most of the feature at 1620–1680 Å are due to He II, rather than to O III]. The latter flux is uncertain, and we can only give a conservative upper limit of ~1.0 times the N III] flux. The best fit in Figure 4 has an O III] flux only ~0.1 times the N III] flux. The peak at ~1780 Å is caused by resonance scattering of Ne III]
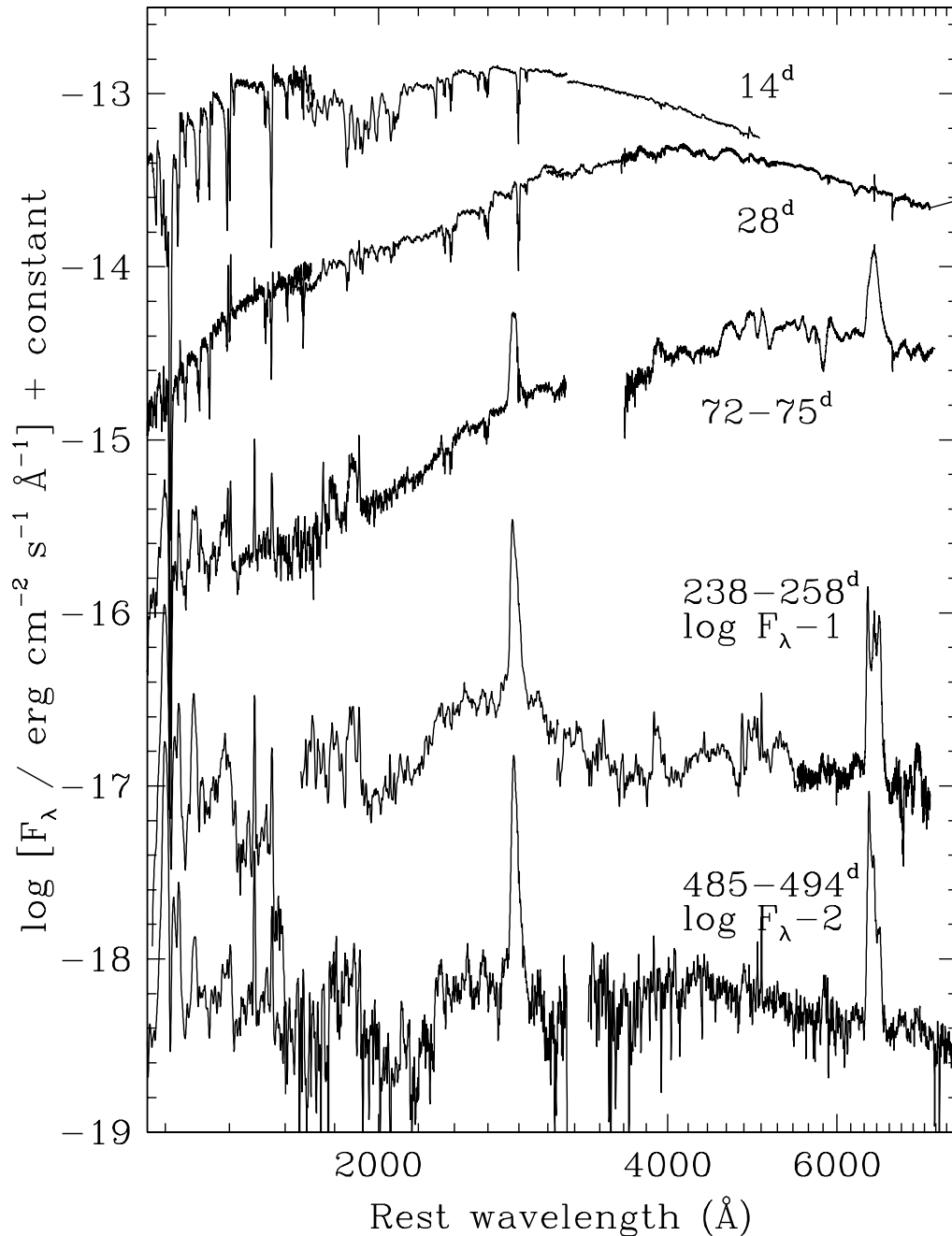
Fig. 5.—Evolution of the spectrum of SN 1998S, with epoch (days after the explosion) indicated. The bottom two spectra are shifted downward by 1 and 2 dex, relative to the previous ones.

We immediately note the difference between the Hα line profile on one hand and Lyα and Mg II on the other hand. While the former line up to the 238–258 day spectrum shows a fairly strong red component, this is missing for the latter. Furthermore, in the day 72–75 spectrum the Hα line is peaked at ~ -1000 km s^{-1} and extends to zero velocity. The flux of both Lyα and Mg II, however, drops close to zero already at ~ 2000 km s^{-1}. As is seen from the earlier spectra, one reason for this difference is likely to be interstellar Lyα and Mg II absorption from our Galaxy and from the host galaxy. Even considering this, the low fluxes in the red wings of Lyα and Mg II make them distinctly different from Hα.

The evolution of the shape of the Hα line has been discussed in several papers (Leonard et al. 2000; Gerardy et al. 2000; Fassia et al. 2001; Pozzo et al. 2004). Our observations, however, cover a longer time interval. In Figure 9 we show the temporal evolution of the Hα line from day 75 to day 2148. From being symmetrical during the first months, as seen in the day 75 spectrum, the line developed a clear asymmetry by day 100, with the blue wing considerably fainter than the red. By day 200 the line again changed character, now with a considerably fainter red wing compared to the blue, as seen in the day 258 spectrum (see also Fig. 4 in Gerardy et al. 2000). This evolution continued, and by day 653 the red wing was almost gone. In the very late spectrum on day 2148 the blue peak had almost disappeared, and instead the central peak was strong. The red part of the line is still much weaker than the blue. The absolute level, however, is uncertain because of the difficulty of an accurate background subtraction.

A central peak is seen in the spectra at several epochs. It is, however, not clear that this peak is of supernova origin. The
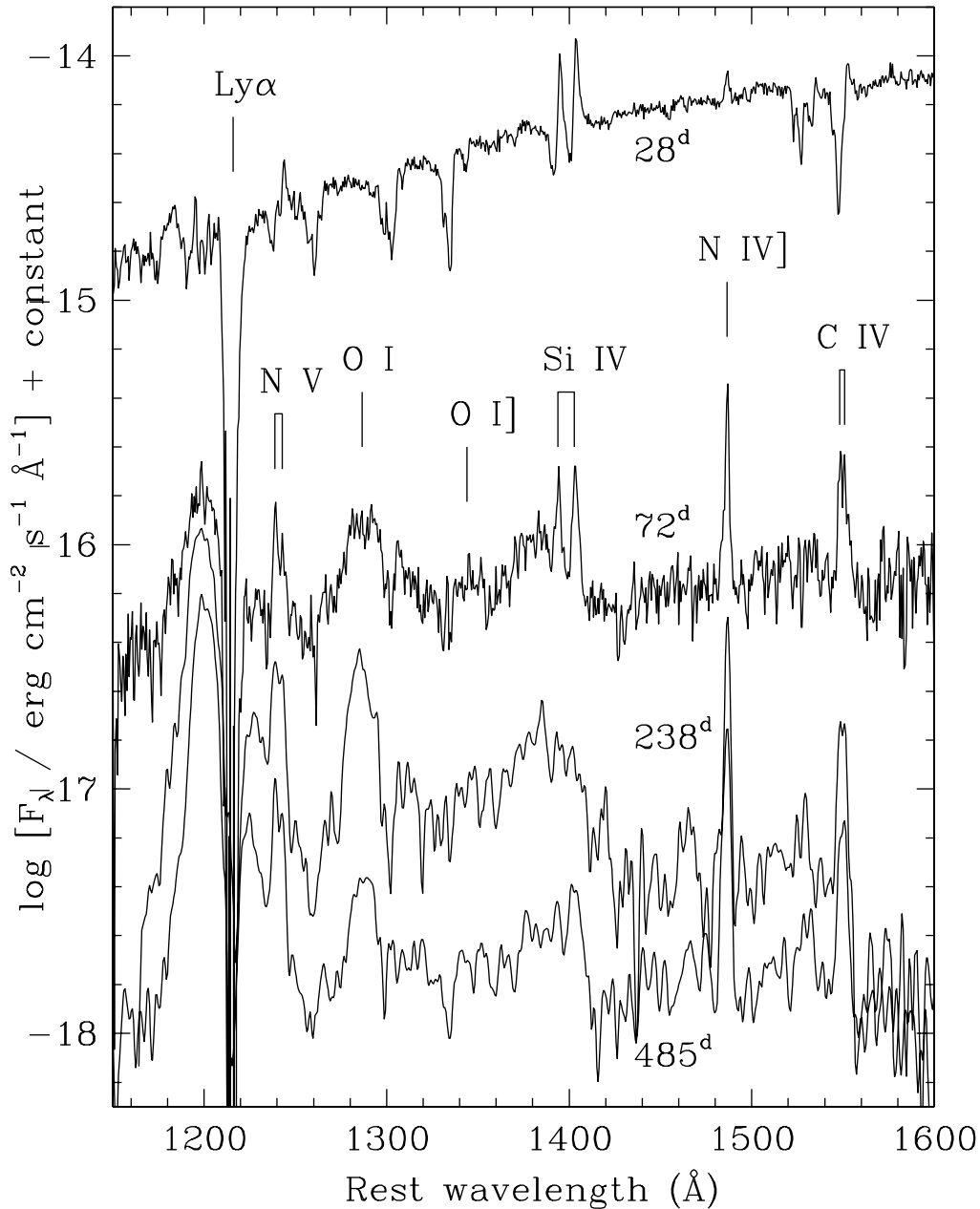
FIG. 6.—Evolution of the far-UV spectrum of SN 1998S from 1998 March 30 to 1999 June 30. Each spectrum is shifted down by 0.5 dex with respect to the previous one.

flux of this peak relative to the rest of the line is sensitive to the subtraction of the background emission from the galaxy, and therefore to the atmospheric seeing. In particular, the reality at the last epochs is questionable. In these the background [N II] $\lambda\lambda6548.0, 6583.5$ lines at -686 and 960 km s^{-1} can clearly be seen, which shows that there is contamination from the background. The fact that a peak is not seen in the Mg II line, observed with *HST*, further strengthens this conclusion.

From Figure 9 we note the clear decrease in the velocity of the blue peak from ~4300–4700 km s^{-1} on days 108–258 to ~3900 km s^{-1} on days 494 and 653. The maximum blue velocity decreases marginally from ~7300 to ~6800 km s^{-1}. In addition to the dramatic change in the line profile, the large Balmer decrement is of special interest, as noted earlier by Leonard et al. (2000), who argue that this strongly implies an origin in gas of very high density.

By day 72 the Mg II line already showed a strong red-blue asymmetry, which persisted throughout the duration of the remaining observations, but there is no indication of a red peak in this line. The Lyα line, however, shows an indication of a red peak in the spectra after day 72. Gerardy et al. (2000) propose that the fading of the red peak relative to the blue can be explained as a result of dust formation. The fact that the red wings of Mg II and Lyα are suppressed earlier than Hα is consistent with this interpretation, as is the dust signature seen in the infrared (Gerardy et al. 2002). For a standard extinction curve, the optical depths at Mg II and Lyα are related to that at Hα by $\tau(\text{Mg II}) = 2.4\tau(\text{H}\alpha)$ and $\tau(\text{Ly}\alpha) = 4.3\tau(\text{H}\alpha)$.

Other broad lines at ~1288, 1344, 1380, 1790, and 1880 Å are less obvious to identify. We note, however, the similar profiles of these lines to that of the Mg II line. Based on the velocity shift of the blue peak, we find that a consistent set of
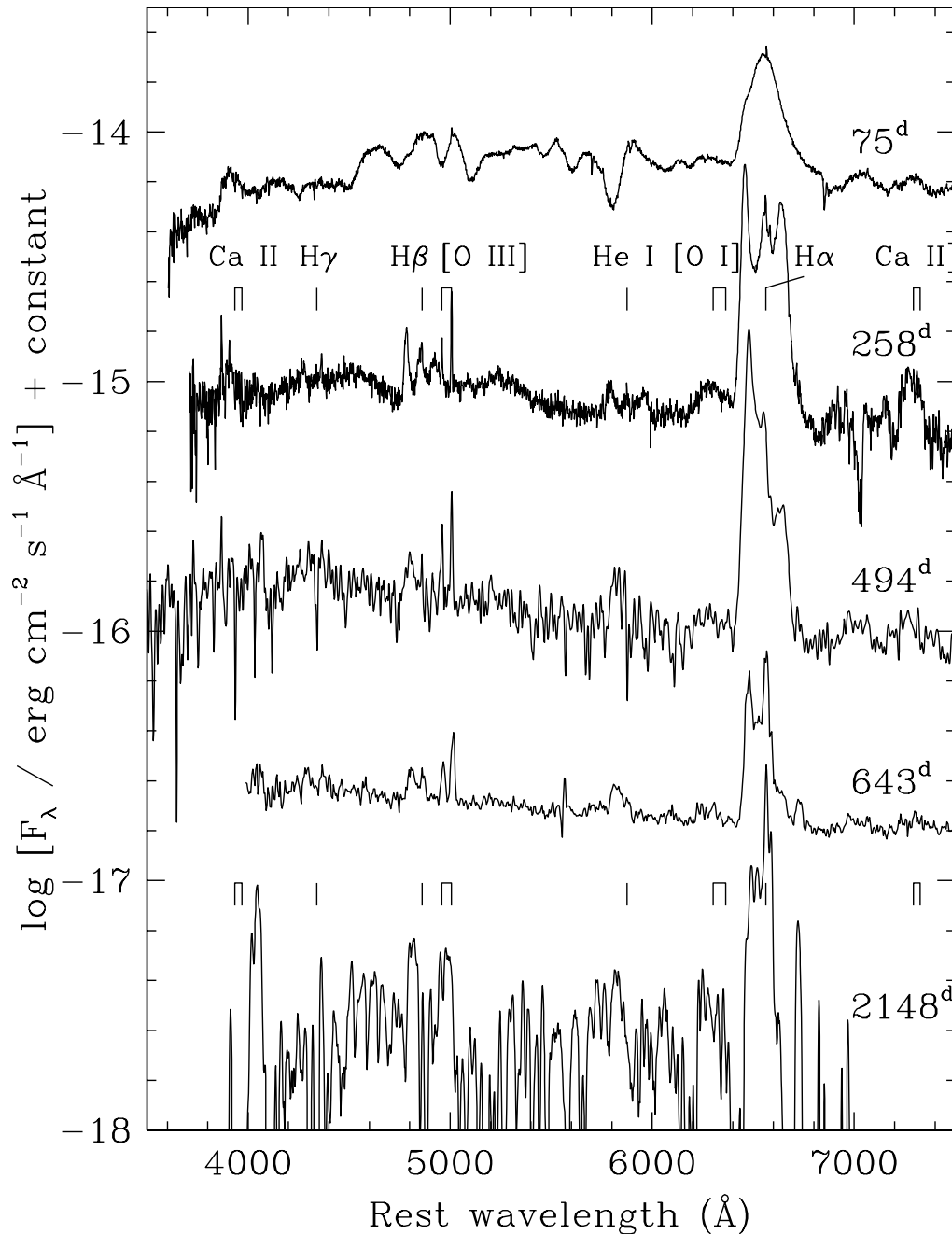
Fig. 7.—Evolution of the optical spectrum of SN 1998S in the nebular phase, where rest wavelengths of the most important lines are marked. The spectra are not calibrated on an absolute scale, but the relative flux calibration within each spectrum is generally reliable. The spectrum at 643 days was taken under bad seeing and is contaminated by background H ii regions, decreasing the contrast of the lines, as well as adding narrow components at the rest wavelength of especially Hα and [O iii] $\lambda\lambda$4959, 5007. Also, the day 2148 spectrum is contaminated by the galaxy background, and we have only been able to make an approximate subtraction of this.

line profiles can be obtained if we identify these lines as O i $\lambda\lambda$1302.2–1306.0, O i $\lambda\lambda$1355.6–1358.5, Si iv $\lambda\lambda$1393.8, 1402.8, [Ne iii] λ1814.6, and C iii] $\lambda\lambda$1906.7–1908.7, respectively. The presence of broad O i lines in the UV is not surprising in view of the broad O i $\lambda\lambda$7771.9–7775.4 features identified by Fassia et al. (2001); both sets of lines probably arise as a result of recombination. We return to the implications of the presence of these lines in § 4.1.

In Figure 10 we show the day 72–75 optical and UV line profiles on a common velocity scale. There is some indication for a broad component of C iv $\lambda\lambda$1548.9, 1550.8, but this is marginal. For N v $\lambda\lambda$1238.8, 1242.8, N iv] λ1486, and N iii] $\lambda\lambda$1746.8–1754.0 there is no evidence for any broad compo-

nents above the noise. From the figure we note that there is marginal evidence for a somewhat smaller extension of the blue wing of Hα (to $\sim$7000 km s^{-1}) compared to Mg ii. The Lyα, C iii], Si iv, and O i lines have velocities consistent with the Mg ii line. The [O i] $\lambda\lambda$6300.3, 6363.8 lines seem to be considerably narrower, but their shape is affected by neighboring lines, as well as by the large separation of the doublet components.

The [O iii] $\lambda\lambda$4958.9, 5006.8 region is similarly complicated by the doublet nature, as well as by the neighboring Hβ line. In the spectra from 75 to 137 days, there is a clear feature at approximately the position of the [O iii] lines (Fig. 7). The peak is $\sim$2000 km s^{-1} redward of the rest wavelength, but this is also approximately the case for Hα. To test this more quantitatively
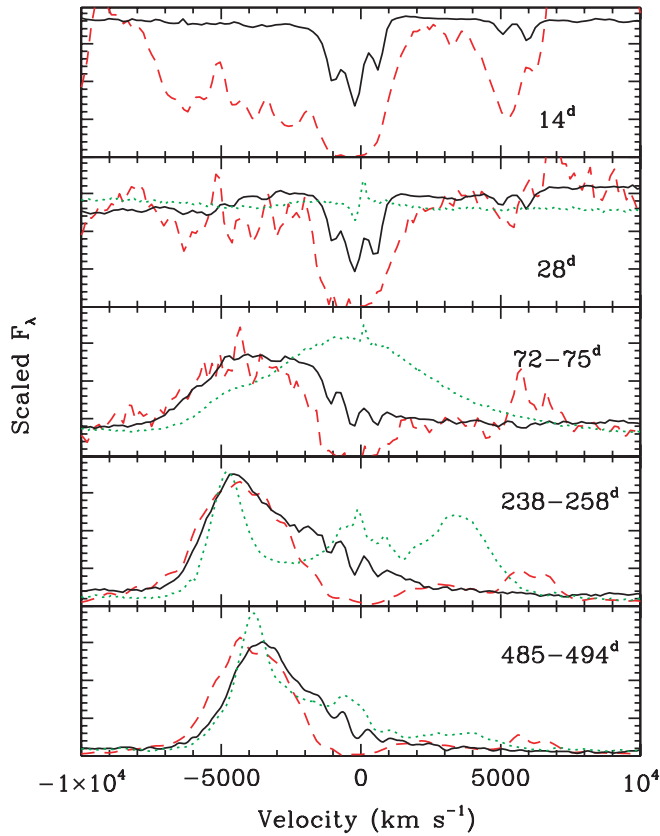
Fig. 8.—Evolution of the Mg II (*solid lines*), Lyα (*dashed lines*), and Hα (*dotted lines*) profiles in SN 1998S from 1998 March 16 (day 14) to 1999 June 30 (day 485). The Hα region was not observed at the first epoch (day 14).

we have used the Hα profile to create a synthetic spectrum, including Hβ and [O III] λλ4958.9, 5006.8, adjusting the line strengths so as to give a best fit to the 4700–5200 Å region. The result of this, however, gives a peak that is too blue, at ~5040 Å. In addition, the [O III] λλ4958.9 component gives a too shallow red wing of the Hβ line. We therefore conclude that the feature at ~5040 Å in the early spectra is unlikely to be due to [O III], but is probably an Fe II line with λ ≈ 5015 Å. In the spectra later than ~300 days there is a faint line at the [O III] wavelength, best seen in the last spectrum at 2148 days, which is most likely from [O III]. The line profile of the [O III] line is, within the errors, similar to that of Hα, with a heavily absorbed red component.

Other lines in the optical spectrum in Figure 7 are discussed by Gerardy et al. (2000), Leonard et al. (2000), Fassia et al. (2001), and Pozzo et al. (2004). We only remark that in our last two spectra on days 643–653 and 2148 we see the same lines as in the earlier spectra, in particular Hβ, He I 5876, [O I] λλ6300, 6364, and [O III] 4959, 5007.

3.2.2. Narrow Lines

Because of the relative lack of blending, the identification and flux measurements of the narrow circumstellar lines are considerably simplified compared to the broad lines. This is particularly true when we compare with the flux measurements of the far-UV lines of SN 1993J, where we had to use a complicated deblending procedure.

In Table 5 we give the fluxes of the narrow lines below 2300 Å. Because of the strong continuum and the influence of P Cygni absorptions of several lines, the day 28 fluxes are uncertain. The noise level of the days 238 and 485 spectra are such that the
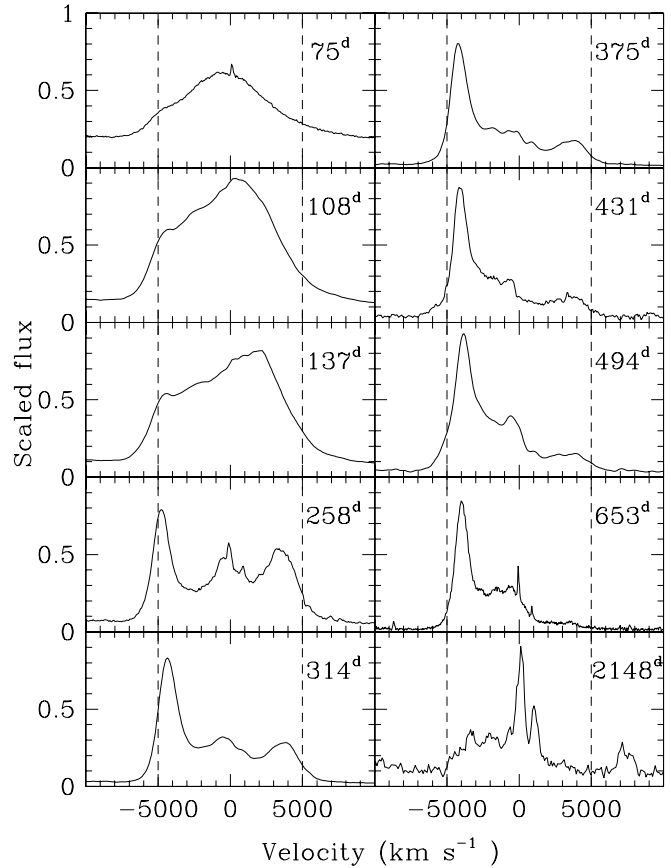

Fig. 9.—Evolution of the Hα line in SN 1998S. The linear flux scale differs among the different dates. The dashed lines mark ±5000 km s⁻¹. Note the progressive decrease in the velocity of the blue peak from ~4500 to ~3900 km s⁻¹.

fluxes are also very uncertain for many of the lines. In the subsequent abundance analysis we therefore restrict ourselves to the day 72 spectrum, which has a suitable combination of high S/N and well-defined emission lines (see Fig. 6).

In Figure 11 we show the day 72 spectrum shortward of 2000 Å in greater detail, together with line identifications. Based on
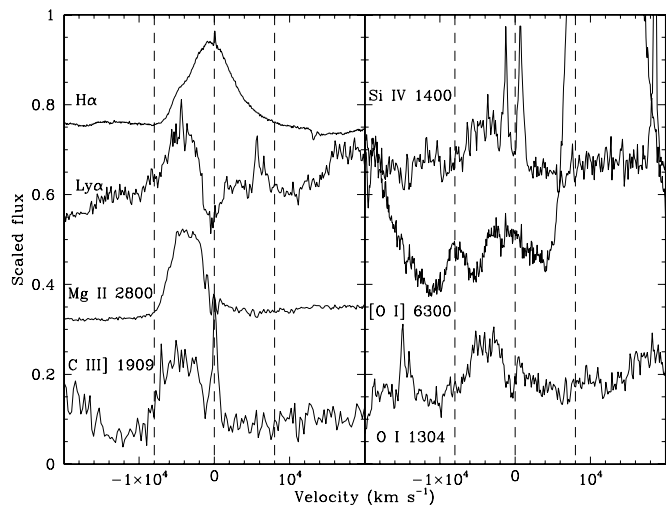

Fig. 10.—Comparison of the SN 1998S line profiles of Hα, Lyα, Mg II, C III], Si IV, [O I], and O I λλ1302.2–1306.0 on day 72. To show the profiles more clearly the flux scale differs among the lines. The dashed vertical lines show a velocity of 0 and ±8000 km s⁻¹ from the rest wavelengths.

TABLE 5
Fluxes of the Narrow Lines in SN 1998S

Line	Rest Wavelength (Å)	Observed Wavelength (Å)	Day 28 (1998 Mar 30)	Day 72 (1998 May 13)	Day 238 (1998 Oct 26)	Day 485 (1999 Jun 30)
N v	1238.8, 1242.8	1238.5 1240.6	3.0:	1.10	1.6	1.4
Si iv	1393.8	1394.0	19.1	0.88	. . .	. . .
Si iv	1402.8	1403.1	26.1	1.27	. . .	. . .
N iv]	1483.3–1487.9	1486.3	5.8	2.49	1.40:	2.16
C iv	1548.9, 1550.8	1549.2	. . .	2.66	0.91	1.03
N iii]	1746.8–1753.4	1751.1	18.2:	2.47	. . .	. . .
C iii]	1906.7, 1909.6	1909.3	36.5:	3.77	1.43	0.41:
C ii]	2322.7–2328.8	2325.0	1.7	1.3	. . .	. . .

Note.—Observed fluxes are in units of 10^{-15} ergs s^{-1} cm^{-2}.

their observed rest wavelengths in the day 72 spectrum, 1394.0 and 1403.1 Å, we identify these lines as coming from Si iv rather than O iv. The FWHM of N iv] λ1486 is consistent with being unresolved, noting that the resolution is ~250 km s^{-1} at this wavelength. High-resolution optical and UV observations during the first month showed two low-velocity components (Fassia et al. 2001; Bowen et al. 2000). While [O iii] λ5006.8, for example, had a FWHM of 50–60 km s^{-1}, the intermediate-velocity Hα absorption component extended to ~350 km s^{-1}. Unfortunately, the limited resolution of our spectra prevents us from relating the narrow emission lines to one or the other of these components. The C iv $\lambda\lambda$1548.9, 1550.8 doublet is clearly resolved in the day 72 spectrum. In addition, the Si iv $\lambda\lambda$1393.8, 1402.8 and the N v $\lambda\lambda$1238.8, 1242.8 doublets are resolved in the same spectrum. The intensity ratio (N v λ1239)/(N v λ1243) is ~1.5. In the region longward of 2000 Å, narrow lines of [N ii] $\lambda\lambda$2139.7, 2143.5 are clearly present, as well as C ii] $\lambda\lambda$2322.7–2328.8.

For the following discussion we note that the uncertainties in the fluxes in the day 72 spectrum are 7%–9% for all lines, except for the N iii] lines (~20%). For the other dates the uncertainties are considerably larger. These values only include the noise, estimated in the neighborhood of each line. In addition, there may be systematic errors originating from the assumed level of the continuum, as well as from line blending; in contrast to SN 1993J, however, these errors are likely to be small because of the well-defined line profiles.

As for SN 1993J, the high noise level in the 1600–1700 Å region prevents us from giving a reliable O iii] λ1664 flux. As an upper limit to the flux we find ~1.5×10^{-15} ergs s^{-1} cm^{-2}.

4. DISCUSSION

4.1. Origin of the Emission Lines

As has been discussed elsewhere (e.g., Chevalier & Fransson 1994, 2003), the origin of the broad lines seen in SN 1993J and
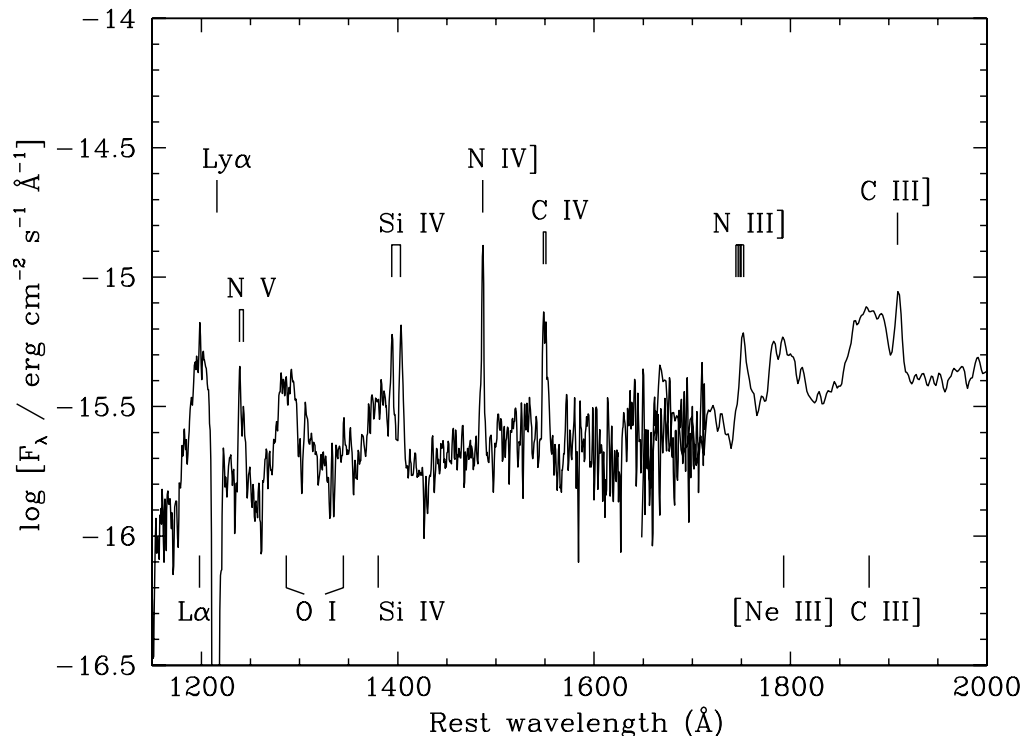
Fig. 11.—Far-UV spectrum of SN 1998S on 1998 May 13 (day 72). Identifications of the narrow lines are given in the top part of the figure (except for Lyα). In the bottom part identifications of the broad lines are given. The lines here show the observed center of the feature, not the rest wavelengths.

SN 1998S can be explained as a result of photoionization by X-rays and UV emission from the radiative reverse shock propagating into the supernova ejecta. The reprocessed radiation from the low-density, unshocked ejecta emerges mainly as UV lines of highly ionized species such as C III–IV, N III–V, and O III–VI. Because of cooling, a dense shell is formed behind the reverse shock—that is, between the reverse shock and the contact discontinuity. The high density in this region causes the reprocessed radiation to emerge mostly as emission from neutral or singly ionized ions, such as H I lines, Mg II, and Fe II.

While the boxlike line profiles in SN 1993J (Fig. 3) are consistent with those coming from a narrow, spherical shell, the geometry of the line-emitting region in SN 1998S is less clear. Gerardy et al. (2000) interpret the double-peaked Hα line profile as a result of the interaction of the ejecta with a circumstellar ring (see also Chugai & Danziger 1994). The centrally peaked profile is explained by a separate component—a spherical distribution of shocked circumstellar clouds. Similar ideas are proposed by Leonard et al. (2000), who relate this picture to a binary scenario, reminiscent of that discussed for SN 1987A.

Although there is no quantitative discussion of this hypothesis, some features in this scenario may be understood from the general picture in Chevalier & Fransson (1994). The broad wings would then represent the emission from the ejecta, while the narrow component is from the shock propagating into the ring, and possibly also the reverse shock, in case this is radiative. Most of the UV and optical line emission is then produced as a result of photoionization of the ejecta, as well as the ring and the cool postshock gas. The ingoing fraction will mainly be absorbed by ejecta gas close to the reverse shock, explaining the ringlike emission also from the ejecta component. The density distribution of the ejecta is likely to be more uniform with respect to polar angle, possibly resembling the nonspherical models of Blondin et al. (1996). We return to this scenario in the next section.

In SN 1995N (Fransson et al. 2002), there was a clear distinction in the line widths of the hydrogen and Mg II lines compared with those of the high-ionization UV metal lines. While the former had smoothly declining line profiles with velocities (HWZI) up to $\sim$10,000 km s^{-1}, the latter were box-shaped, with HWZI $\approx$ 5000 km s^{-1}. No such distinction is obvious for either SN 1993J or SN 1998S.

The strong O I recombination lines present in SN 1998S resemble those seen in SN 1995N. In Fransson et al. (2002), it was argued that in order to explain their strengths relative to the hydrogen lines, they had to originate in processed gas with a high abundance of oxygen. We believe the same is true for SN 1998S, which indicates that some of the gas giving rise to the broad metal lines comes from processed gas. SN 1993J also has strong metal lines in the UV, as well as in the optical, which grow stronger with time relative to Hα (Matheson et al. 2000b). Hence, there cannot be a large mass of hydrogen present between the reverse shock and the oxygen-rich core. It is likely that SN 1993J, SN 1995N, and SN 1998S had lost most of their hydrogen-rich gas, and the helium and oxygen core is therefore efficiently illuminated by the X-rays from the reverse shock.

The origin of the relatively narrow lines seen in SN 1998S, and in other SNe IIn, is less clear. Given their small velocity width, they must arise in circumstellar gas. This can be either unshocked gas in front of the shock, or dense regions shocked by the blast wave.

4.2. Asymmetrical Hα Emission and Dust Formation in SN 1998S

As mentioned in § 1, there are several indicators of dust present in SN 1998S, both from the line profiles and from the strong infrared excess (Gerardy et al. 2002; Pozzo et al. 2004). In addition, the double-peaked line profiles provide a very interesting clue to the nature of the line-emitting region. Gerardy et al. (2000), in particular, attribute this to emission by a torus-like region. In this section we discuss the dust and the geometry of the line-emitting region.

The location and nature of the dust is not clear. An obvious candidate is dust formed in the heavy-element–enriched ejecta. If most of the line emission comes from a shell close to the reverse shock, the dust in the core will primarily absorb the high-velocity emission from the receding ejecta, in agreement with the observations. This is the scenario favored by Gerardy et al. (2000) for the asymmetrical line profiles. Gerardy et al. (2002), however, find that the same dust cannot explain the excess emission seen in the infrared. Instead, they attribute this to an echo from preexisting dust.

Another interesting possibility is that the dust absorption, as well as the emission, takes place in the cool dense shell (CDS) in the shock region (Deneault et al. 2003). This is a favorable place for dust formation because of its high density and low temperature (Fransson 1984b; Chevalier & Fransson 1994). Whether it is cool enough, given the X-ray heating from both shocks, remains to be demonstrated quantitatively. The fact that the gas swept up by the shocks may be enriched by heavy elements may be important in this context. Indications for metal enrichment in SN 1998S are also presented from X-ray observations by Pooley et al. (2002). The temperature of the emission should be close to the condensation temperature, which agrees with the Gerardy et al. (2002) temperature estimate of the dust emission, 700–1400 K. Recently, Pozzo et al. (2004) find that the luminosity and temperature of the IR emission gives a blackbody radius corresponding to a velocity of $\sim$4000 km s^{-1} at 330–400 days. This is comparable to the velocity of the blue and red peaks of the Hα line at this time. Later, the blackbody velocity of the dust recedes to $\sim$1000 km s^{-1}, indicating a thinning of the dust.

A problem with this idea is that the dust is likely to condense behind the zone relative to the reverse shock where Hα, Mg II, and other low-ionization lines are formed. If the CDS is formed behind the reverse shock (in the Lagrangian sense), this means that both the front- and back-side line emission will be absorbed by the dust, contrary to the observations. A solution to this may come from the fact that hydrodynamic mixing may give rise to a clumpy CDS (Chevalier & Blondin 1995). This could lead to a covering factor of the dust less than unity and allow some of the Hα to penetrate.

An alternative, related possibility, discussed for SN 1993J by Fransson et al. (1996), is that the forward shock is radiative. In this case the line emission from the receding part of the shell (red wing) will be absorbed by the dust shell, while the line emission from the front (blue wing) can emerge freely. Although dismissed for SN 1993J, a high circumstellar density, as may be the case for SN 1998S, may make this a real possibility. Alternatively, there may be a combination of ejecta dust absorption and emission from dust created in the CDS. The latter then has to be either clumpy or optically thin, in order to not block the line emission from the shell.

Finally, we note that emission from perhaps 2–4 $M_\odot$ of cold dust from Cas A has recently been claimed by Dunne et al. (2003). This estimate of the amount of dust, however, has been questioned by Dwek (2004), who finds that a more reasonable mass of only 10^{-4} to 10^{-3} $M_\odot$ is needed, if the dust is in the form of conducting, metallic needles. This illustrates the sensitivity of the mass estimate to the nature of the dust. But the
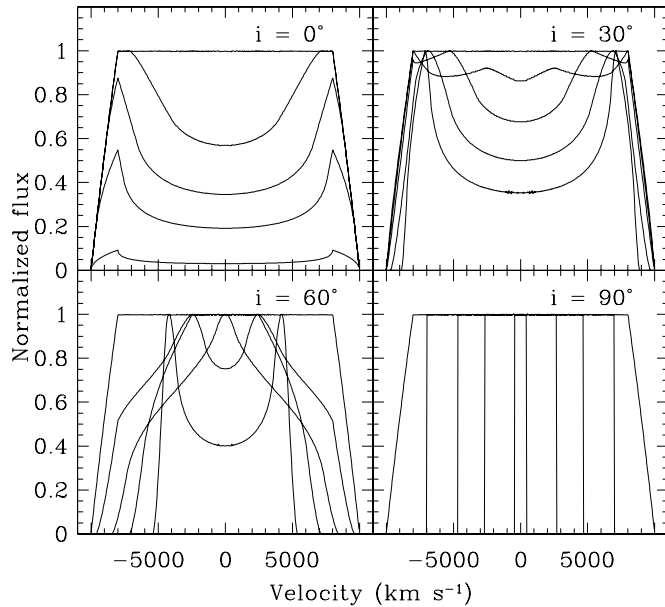
FIG. 12.—Line profiles for a uniformly emitting torus for four different values of the inclination i and for different values of the angular thickness of the torus, $\theta = 5°$, $30°$, $50°$, $70°$, and $90°$. In the top two panels, the flux at $v = 0$ is progressively higher as θ increases. In the bottom two panels, the wings of the line go to progressively higher velocities as θ increases. No dust absorption is included.

FIG. 13.—Line profiles, including dust absorption, for different values of the angular thickness of the torus for $i = 60°$, $V_{in} = 8000$ km s^{-1}, and $V_{out} = 10,000$ km s^{-1}. The dust has been assumed to be inside the Hα-emitting torus, with a covering factor $f_c = 0.5$. Note the transition from a centrally peaked profile to a double-peaked profile as the thickness of the torus decreases.

most interesting result of Dunne et al. (2003) is that the dust emission in Cas A is concentrated in the region between the reverse and forward shocks. This is consistent with the scenario above, where the dust is formed in the CDS during the first years after the explosion.

To study the different scenarios for the dust absorption above in more detail, as well as the effects of an asymmetrical Hα emission, we have calculated several models for the line profiles. In particular, we have considered the different possibilities discussed above for the location of the dust-absorbing region.

To explain the double-peaked nature of the Hα line, we assume in this section that the emission originates in a torus-like region, similar to that proposed by Gerardy et al. (2000). Some support for this also comes from the polarization data for SN 1998S presented by Leonard et al. (2000). This region is characterized by the inner and outer velocities (V_{in} and V_{out}), the angular thickness from the equatorial plane (θ), and the inclination of the torus relative to the line of sight (i, where $i = 90°$ is an edge-on torus). We assume the emissivity within this region to be constant in both the radial and polar directions. The line is assumed to be optically thin.

To model the dust absorption we consider three different locations, either inside the ejecta, behind the reverse shock, or behind the circumstellar shock. We assume the dust to be opaque, but vary the total areal covering factor, f_c.

In Figure 12 we first show line profiles without absorption, but at four different inclination angles ($i = 0°$, $30°$, $60°$, and $90°$) and for several values of the angular thickness from the equatorial plane of the torus. We see here that widely different line profiles may result, depending on the inclination and angular thickness of the torus. In particular, both double-peaked profiles and centrally peaked profiles may arise—the former mainly at low inclinations, while the latter occur for high inclinations and high angular extent of the torus.

By varying the angular thickness of the torus we can create a sequence of line profiles, which approximately resembles the
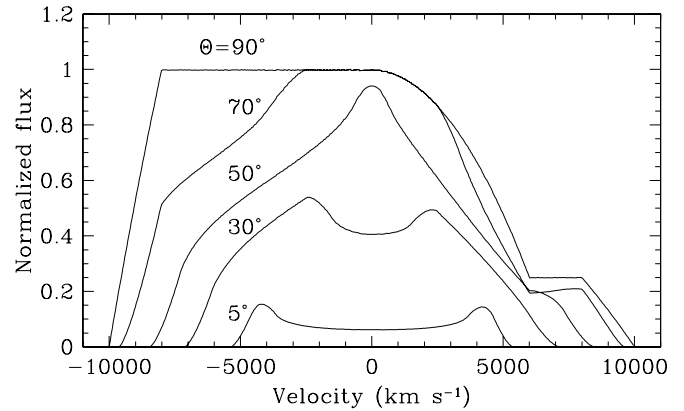
observed evolution of the Hα line. In principle, one could therefore think of an evolutionary time sequence from a large angular thickness to a smaller one. This could, for example, result from the interaction of the supernova with a flattened circumstellar environment, of which a thick disk is the most extreme example. As the supernova expands, the angular extent of the torus would then decrease, and the above evolution in θ would result. We believe this to be the most promising of the torus models.

To this emission we can now add dust absorption according to the various possibilities discussed above. The cases with dust absorption outside of the Hα-emitting region all have the problem that the red wing is considerably stronger than the blue wing. This conclusion is independent of the inclination, the angular thickness, and the covering fraction of the dust. Because this is in contradiction to the observations, we do not further consider these cases.

If we instead assume that the dust absorption occurs inside of the Hα-emitting region, as would be the case for a radiative forward shock, the line profiles are more similar to those observed. As an example, we show in Figure 13 a model with $V_{in} = 8000$ km s^{-1}, $V_{out} = 10,000$ km s^{-1}, $i = 60°$, $f_c = 0.5$, and different values of the angular extent $5° < \theta < 90°$. The line profile with $\theta \approx 60°$ has an approximate resemblance to the Hα profiles on days 75–137 in Figure 9, while the profiles at the later epochs resemble those of smaller θ.

A major problem with this picture, however, is that the extent in velocity of the blue wing is expected to decrease by a factor of about 2 with time during this evolution, as shown in Figure 13. The reason is simply that the velocity along the line of sight decreases as the thickness decreases and is difficult to avoid. In addition, the extent of the flat, weak red wing is difficult to reproduce in this model.

Finally, we consider the case with absorption from dust formed in the ejecta. A total obscuration by this dust is not compatible with the presence of a weak, but finite red wing of the lines. A partial dust obscuration, such as the one in SN 1987A (Lucy et al. 1991) is, however, both more realistic and compatible with the observations. To explain the temporal evolution from a centrally peaked profile to a double-peaked profile, we must refer to a situation similar to that in Figure 13. Although the red part of the line may be better reproduced by this configuration, it has the same problem with a too rapidly decreasing line width as the model above. In addition, it is difficult to reproduce the central peak without an additional component,

such as the one invoked by Gerardy et al. (2000). The reality of this peak is, however, not clear.

In summary, we find it difficult to reproduce the observed evolution of the line profiles with an emitting region in the form of a torus. This is independent of the dust absorption, although more complicated models cannot definitely be ruled out.

4.3. Line Formation in the CDS

While the line profiles of the broad lines in SN 1998S are very clear cases of double-peaked profiles, this also applies to the Lyα, Mg II, and Hα lines in SN 1993J (see Fig. 2). In the case of SN 1993J there are no indications of major nonspherical structures. On the contrary, VLBI imaging shows a basically spherical shell (Marcaide et al. 1997; Bietenholz et al. 2001), which excludes a flattened structure unless we are very close to the axis of symmetry. Therefore, the torus model for the peaks in the line profile is, in the case of SN 1993J, also unlikely for this reason.

An alternative explanation, applying to both SN 1993J and SN 1998S, is based on the fact that both the Lyα and Mg II lines are resonance lines and therefore optically very thick. This is in most cases also true for Hα (Chevalier & Fransson 1994). If, in addition, the line-emitting region is geometrically sufficiently thin, the Sobolev approximation will break down and photons from the emitting shell may be absorbed locally, giving rise to a tilted or double-peaked line (e.g., Rottenberg 1952; Kunasz & Hummer 1974; Bertout & Magnan 1987; Cid Fernandes & Terlevich 1994). Because both the hydrogen and Mg II lines are likely to be dominated by emission from the narrow CDS between the reverse shock and the contact discontinuity (see § 4.1), this region may be too narrow for the Sobolev approximation to be valid.

Bertout & Magnan (1987) have discussed this case and find that "M-shaped" profiles result if three conditions are met: (1) The medium must be optically thick in the line. (2) The shell must be thin enough for the velocity *gradient* over the shell to be small compared to the thermal velocity. (3) The macroscopic velocity must be larger than the thermal velocity. The reason for the high-velocity peaks may be traced back to the fact that the projected area contributing to a frequency interval $[\nu, \nu + d\nu]$ in this limit is proportional to $|\nu - \nu_0|$, where ν_0 is the rest frequency of the line.

As we discuss above, the first of these conditions is true for Lyα and Mg II, and in most cases also for Hα. The second condition is interesting. Lines coming from the ejecta, for example, are generally formed over a fairly large velocity range (Chevalier & Fransson 1994) and are therefore expected to have flat-topped profiles. Lines coming from the CDS, on the other hand, arise in a very narrow shell, no larger than a few times 10^{12} cm (Chevalier & Fransson 1994). If we assume that $v \propto r$ (which is not strictly valid in the CDS, but will provide a conservative estimate), a velocity gradient equal to the thermal velocity ($v_{\rm th}$) corresponds to a distance

$$\Delta r_{\rm th} \approx v_{\rm th} \partial r / \partial v \approx R_{\rm CDS} v_{\rm th} / V_{\rm CDS} = v_{\rm th} t$$
$$\approx 10^{13} (t/100 \text{ days}) \left(T_e / 10^4 \text{ K}\right)^{1/2} A^{1/2} \text{ cm}.$$

Here A is the atomic weight of the ion, $R_{\rm CDS}$ is the radius of the CDS, and T_e is the electron temperature in the CDS. Therefore, the velocity gradient in the CDS is likely to be small enough for the second condition to be valid. This may, however, vary from case to case, as well as over time. A "microturbulence" in the

shell should have the same effect. Condition (3) is fulfilled in all interesting cases. Double-peaked line profiles can therefore be expected in cases where the CDS is sufficiently narrow.

The fact that the Hα line in SN 1998S evolves from a centrally peaked line profile (before $\sim$100 days) to the double-peaked profile at late epochs may be a result of the fact that the width of the CDS at early epochs was large enough for the Sobolev case to apply (note that $\Delta r_{\rm th} \propto t$). In this case, a nearly constant velocity in the shell implies a parabolic line profile.

We therefore conclude that it is likely that *the double-peaked profiles in SN 1998S and, to a less dramatic extent SN 1993J, arise as result of the extremely small thickness of the CDS, in combination with a high optical depth*. Because the width of the CDS is a function of the mass-loss rate and reverse-shock velocity (Chevalier & Fransson 1994), the line profiles provide a useful diagnostic of the conditions behind the reverse shock.

The asymmetry of the red and blue wings of the lines may be caused by either dust or bound-free absorption by the Balmer and Paschen continua from the ejecta and circumstellar interaction region, as discussed in § 4.2. In the latter case, the larger asymmetry for the Mg II line compared to Hα in SN 1993J would then be a result of the larger optical depth in the Balmer continuum. Dust absorption from the same region would have the same effect. While bound-free absorption should decrease with decreasing wavelength, dust absorption would increase. This could be checked by comparison with the [N II] $\lambda\lambda2139.7$, 2143.5 profile. Unfortunately, there are no observations of SN 1993J in the far-UV region on day 670, when the Mg II asymmetry is largest. Given that there is strong evidence for dust emission, the dust interpretation seems most likely.

The origin of the central peak, if coming from the supernova rather than the background H II regions, is not clear. Gerardy et al. (2000) suggested emission from shocked circumstellar clumps, but it may also be possible to explain it as an effect of the line formation process in the cold, dense shell.

We remark that this model does not naturally explain the polarization seen in SN 1998S (Leonard et al. 2000; Wang et al. 2001). The origin of this may, however, be in the density distribution of the ejecta inside of the interaction region. A nonspherical cold dense shell, giving rise to the polarization, would also be compatible with the line profile.

4.4. CNO Ratios in SN 1993J and SN 1998S

The strong N III] and N IV] lines in both SN 1993J and SN 1998S indicate nitrogen enrichment in the supernova ejecta and in the circumstellar gas. To quantify this we make a nebular analysis similar to that in Fransson et al. (1989). Assuming that the ionization zones of the corresponding C and N ions coincide, which is reasonable (see Fransson 1984b; Fransson et al. 1989 and references therein), one can calculate the N III/C III and N IV/C IV ionic ratios as a function of temperature and density. Because reasonable densities are considerably less than the critical values for these ions ($\lesssim 10^9$ cm^{-3}), the density is unimportant for the result. Further, because of the similar excitation potentials of these lines, the temperature is only of minor importance (see below). For the calculations below we use a temperature of 2×10^4 K and an electron density of 10^6 cm^{-3}. In the analysis we have used collision strengths and transition probabilities from the compilation by Pradhan & Peng (1995). For SN 1998S we have used a reddening of $E_{B-V} = 0.23$ mag, and for SN 1993J $E_{B-V} = 0.2$ mag (Richmond et al. 1994; Leonard et al. 2000).

For SN 1998S we find N III/C III = 5.1 ± 1.1 and N IV/C IV = 6.4 ± 0.8, where the errors have been estimated from the

TABLE 6
Temperature and Density Correction Factors

Temperature (K)	Density (cm^{-3})	N III/C III	N IV/C IV	N III/O III
10,000............	10^6	1.16	1.09	0.70
15,000............	10^6	1.04	1.02	0.88
20,000............	10^4	1.04	1.00	1.06
20,000............	10^6	1.00	1.00	1.00
20,000............	10^8	0.96	1.00	0.93
30,000............	10^6	0.95	1.00	1.16

TABLE 7
Summary of CNO Abundances in SNe II

Supernova	Type	Environment	N/C	N/O	Notes
SN 1979C	II-L	Ejecta	8	>2	...
SN 1987A	II-P	Circumstellar	7.8	1.6	Nebular analysis
	...	...	5.0	1.1	Photoionization model
SN 1993J..........	IIb	Ejecta	12.4	>0.8	...
SN 1995N	IIn	Ejecta	3.8	0.2	Uncertain
SN 1998S.........	IIn	Circumstellar	6.0	>1.4	...

uncertainties given in § 3.2.2 and do not include systematic errors. From the O III] limit, we find a lower limit of N III/O III > 1.4. In Table 6, we give the correction factors for these ionic ratios for other temperatures and densities. We see that these never exceed 20% and are therefore of the same order as the uncertainties in the flux measurements.

For the N/C ratio we take a weighted average of the N III/C III and N IV/C IV ratios and obtain N/C = 6.0 ± 0.7. In addition, there are systematic errors from the uncertainty in the temperature and the differences in the extents of the ionization zones. From Table 6, the former can be estimated to be at most 15%. The ionization structure depends on the ionizing source, which may be either the X-rays from the shock wave, or possibly the flux in connection to the breakout of the shock through the photosphere, similar to the situation for the ring of SN 1987A. In that case Lundqvist & Fransson (1996) found that a detailed time-dependent photoionization model resulted in N/C and N/O ratios that were ∼35% lower than those resulting from a simple nebular analysis along the lines in this paper. As a realistic estimate of the N/C ratio, we therefore take N/C = 6.0 ± 2.

Similarly, we obtain for SN 1993J from the N III]/C III] ratio in Table 4 the value N III/C III = 12.4. From the lower limit of the N IV] λ1486/C IV λλ1548.9, 1550.8 ratio of 1.5 we obtain N IV/C IV > 10.2, which is compatible with the N III/C III ratio. We therefore take N/C = 12.4. The limit of N III] λλ1746.8–1754.0/O III] λλ1660.8, 1666.2 > 1.0 translates into N III/O III > 0.8, which we also take as a limit to the N/O ratio. As we pointed out in § 3.1, the feature at ∼1640 Å is more compatible in wavelength with He II λ1640 than with the O III] line, and it is therefore likely that the N/O ratio is larger than the lower limit given above.

Because of the complex deblending procedure in SN 1993J, as well as its lower S/N, the errors in abundances are larger than for SN 1998S, and we estimate that these may be ±50%; thus, N/C = 12.4 ± 6 and N/O > 0.8.

To illustrate the level of carbon depletion in SN 1993J, we have calculated a synthetic spectrum with solar ratios of C, N, and O. This is shown as the dashed line in Figure 4, where we have kept the N III] flux at the same level. The flux of the C III] line has increased by a factor ∼20.

4.5. Comparison with CNO Processing in Other Supernovae

CNO abundance ratios have now been measured for a number of SNe. SN II-L 1979C was the first supernova shown to exhibit enhanced nitrogen abundances; Fransson et al. (1984) find N/C = 8 ± 3 and N/O > 2. The best-studied case to date is the ring of SN 1987A, from which narrow emission lines of C III–IV, N III–V, and O III–IV were observed. Using a nebular analysis similar to the one presented in this paper, Fransson et al. (1989) found that N/C = 7.8 ± 4 and N/O = 1.6 ± 0.8.

Their analysis was later improved using a self-consistent model of the ring emission, yielding N/C = 5.0 ± 2.0 and N/O = 1.1 ± 0.4 (Lundqvist & Fransson 1996). The discrepancy between these abundance ratios gives a reasonable estimate of the systematic errors due to differences in the ionization zones, as well as the temperature of the gas. SN 1995N was the first SN IIn to have a C/N ratio determined from a spectral analysis of broad ejecta lines similar to that of SN 1979C and SN 1993J. In Table 7, we summarize CNO ratios for SN 1979C, SN 1987A, SN 1993J, SN 1995N, and SN 1998S. Because of blending, the broad-line determinations are affected by a larger uncertainty, compared to values from the narrow circumstellar emission lines in SN 1987A and SN 1998S. This applies especially to SN 1995N.

From Table 7 we see that in all cases where CNO abundances have been measured, the N/C ratio is considerably larger than the solar value, N/C = 0.25 (Grevesse & Sauval 1998). The N/O ratio is more uncertain because of the problems with O III] λ1664. The only well-determined case is SN 1987A, where N/O ≈ 1.1, again much larger than the solar value N/O = 0.12.

All supernova progenitors in Table 7 are believed to have undergone extensive mass loss prior to the explosion. Models of SN 1987A suggest that ∼6 $M_\odot$, out of the original ∼14 $M_\odot$ hydrogen envelope mass, were lost before the explosion (e.g., Shigeyama & Nomoto 1990). This may be characteristic for Type II-P progenitors, although one should keep in mind that the SN 1987A progenitor was not typical for a Type II-P and that the progenitor mass was relatively high. For the other Type II subclasses, Nomoto et al. (1995) have proposed a binary scenario, where the SNe II-L and SNe IIn have lost a moderate amount of the hydrogen envelope, while SNe IIb have an envelope mass ≲1 $M_\odot$. Type Ib and Ic SNe have lost all of their hydrogen envelope and, in the case of SNe Ic, also the helium mantle. As we discussed in § 4.1, for SN 1993J, SN 1995N, and SN 1998S there is strong evidence that the progenitors had lost most of their hydrogen envelopes before the explosion.

With this background, it is tempting to see the nitrogen enrichment in these SNe as being a result of this mass loss. A more quantitative comparison is, however, not straightforward. Stellar evolutionary models of massive stars, including effects of mass loss, rotation, and binarity, have been calculated by several groups. In particular, rotation can have a large effect on the CNO abundances by increasing the mixing from the CNO burning region already in the main-sequence phase (Meynet & Maeder 2000; Heger & Langer 2000). Binary mass exchange produces a result that, unfortunately, is not easily distinguished from that of rotation (Wellstein & Langer 1999).

The nitrogen enrichment in SN 1987A has put considerable constraints on progenitor models (for reviews, see Podsiadlowski 1992; Woosley et al. 2002). Here the problem is to explain the blue progenitor, the red-to-blue supergiant ratio in the LMC, and the CNO ratios in a consistent model. To fulfill all these

constraints has turned out to be difficult in single-star scenarios. For example, Saio et al. (1988) had to artificially invoke complete mixing of the hydrogen envelope.

Hillebrandt & Meyer (1989), Podsiadlowski et al. (1990), and Ray et al. (1993) have argued that binary models, in particular merger models, should be more successful in these respects. The nitrogen enrichment is then a natural consequence of the merger or accretion process, which adds both angular momentum and energy; this may in turn induce large-scale mixing of the envelope. In addition, the triple-ring structure may be more naturally explained in this kind of scenario. A problem may be that such models require some fine tuning of the precise epoch when the merger takes place (see, e.g., Woosley et al. 2002).

Of the remaining SNe, the N/C ratio of SN 1993J may be the easiest one to explain. Light-curve calculations (Nomoto et al. 1993; Woosley et al. 1994) and spectral models (Patat et al. 1995; Houck & Fransson 1996) have shown that the hydrogen envelope of SN 1993J must have had a mass of less than 1 $M_\odot$ at the time of the explosion. For this to occur without too much fine tuning, a binary model is most natural. Both of these properties make the mixing of CNO-processed products to the surface natural.

Nitrogen enrichment has also been found in older supernova remnants, most notably in Cas A. Chevalier & Kirshner (1978) discovered an overabundance of nitrogen by an order of magnitude in the quasi-stationary flocculi, presumably originating from the clumpy wind of the progenitor. Lamb (1978) explained this enrichment as a result of CNO burning in combination with mass loss from a progenitor of 15–25 $M_\odot$. Moreover, Fesen & Becker (1991) and Fesen (2001) identified fast-moving knots rich in both hydrogen and nitrogen. Some of these were found outside the main blast wave. These must have been expelled from the photosphere of the progenitor at the time of the explosion, showing that the progenitor had at least a thin nitrogen-enriched hydrogen envelope. Based on these observations Chevalier & Oishi (2003) have suggested that the progenitor of Cas A was a Type IIb or IIn supernova. The broad wings seen in Hα for both SN 1998S and SN 1995N (Fransson et al. 2002) may have originated in comparable high-velocity clumps, which have penetrated the supernova blast wave. The narrow

component may be similar to the quasi-stationary flocculi. Finally, for Cas A we have already noted the possibility of a similar scenario for the dust formation as for SN 1998S.

5. CONCLUSIONS

The most important result of the observations presented here is the strong indication of nitrogen enrichment in both SN 1993J and SN 1998S. This, together with similar evidence from other SNe II, puts strong constraints on their progenitors. The CNO enrichment also gives independent support for mass loss from the progenitors. The line profiles and the presence of high-ionization lines are direct indicators of the ionizing effects from the reverse shock wave, in qualitative agreement with that expected from models of circumstellar interaction. The double-peaked nature of the line profiles is interpreted as a result of the emission from the CDS behind the reverse shock, rather than a torus, and can serve as an important diagnostic of the former. The quantitative features of this, however, remain to be demonstrated. From the asymmetry of the line profiles in SN 1998S, we find additional support for dust formation in the ejecta.

REFERENCES

Barbon, R., Benetti, S., Cappellaro, E., Patat, F., Turatto, M., & Iijima, T. 1995, A&AS, 110, 513
Baron, E., Hauschildt, P. H., & Branch, D. 1994, ApJ, 426, 334
Bertout, C., & Magnan, C. 1987, A&A, 183, 319
Bietenholz, M. F., Bartel, N., & Rupen, M. P. 2001, ApJ, 557, 770
Blondin, J. M., Lundqvist, P., & Chevalier, R. A. 1996, ApJ, 472, 257
Bowen, D. V., Roth, K. C., Meyer, D. M., & Blades, J. C. 2000, ApJ, 536, 225
Chevalier, R. A., & Blondin, J. M. 1995, ApJ, 444, 312
Chevalier, R. A., & Fransson, C. 1994, ApJ, 420, 268
———. 2003, in Supernovae and Gamma-Ray Bursts, ed. K. W. Weiler (New York: Springer), 171
Chevalier, R. A., & Kirshner, R. P. 1978, ApJ, 219, 931
Chevalier, R. A., & Oishi, J. 2003, ApJ, 593, L23
Chugai, N. N. 2001, MNRAS, 326, 1448
Chugai, N. N., & Danziger, I. J. 1994, MNRAS, 268, 173
Chugai, N. N., et al. 2004, MNRAS, 352, 1213
Cid Fernandes, R. C., & Terlevich, R. 1994, in Violent Star Formation: From 30 Dorados to QSOs, ed. G. Tenorio-Tagle (Cambridge: Cambridge Univ. Press), 365
de Boer, K. S., Pascual, P. R., Wamsteker, W., Sonneborn, G., Fransson, C., Bomans, D. J., & Kirshner, R. P. 1993, A&A, 280, L15
Deneault, E. A.-N., Clayton, D. D., & Heger, A. 2003, ApJ, 594, 312
Dunne, L., Eales, S., Ivison, R., Morgan, H., & Edmunds, M. 2003, Nature, 424, 285
Dwek, E. 2004, ApJ, 607, 848

Fabricant, D., Cheimets, P., Caldwell, N., & Geary, J. 1998, PASP, 110, 79
Fassia, A., et al. 2000, MNRAS, 318, 1093
———. 2001, MNRAS, 325, 907
Fesen, R. A. 2001, ApJS, 133, 161
Fesen, R. A., & Becker, R. H. 1991, ApJ, 371, 621
Fesen, R. A., et al. 1999, AJ, 117, 725
Filippenko, A. V. 1982, PASP, 94, 715
———. 1997, ARA&A, 35, 309
Filippenko, A. V., & Matheson, T. 2004, in Supernovae: 10 Years of SN 1993J, ed. J. M. Marcaide & K. W. Weiler (New York: Springer), in press
Filippenko, A. V., Matheson, T., & Barth, A. J. 1994, AJ, 108, 2220
Filippenko, A. V., Matheson, T., & Ho, L. C. 1993, ApJ, 415, L103
Finn, R. A., Fesen, R. A., Darling, G. W., Thorstensen, J. R., & Worthey, G. S. 1995, AJ, 110, 300
Fransson, C. 1984a, A&A, 132, 115
———. 1984b, A&A, 133, 264
Fransson, C., Benvenuti, P., Wamsteker, W., Gordon, C., Hempe, K., Reimers, D., Palumbo, G. G. C., & Panagia, N. 1984, A&A, 132, 1
Fransson, C., Cassatella, A., Gilmozzi, R., Kirshner, R. P., Panagia, N., Sonneborn, G., & Wamsteker, W. 1989, ApJ, 336, 429
Fransson, C., Lundqvist, P., & Chevalier, R. A. 1996, ApJ, 461, 993
Fransson, C., & Sonneborn, G. 1994, in Frontiers of Space and Ground-Based Astronomy, ed. W. Wamsteker, M. S. Longair, & Y. Kondo (Dordrecht: Kluwer), 249
Fransson, C., et al. 2002, ApJ, 572, 350

Freedman, W. L., et al. 1994, ApJ, 427, 628
Gerardy, C. L., Fesen, R. A., Höflich, P., & Wheeler, J. C. 2000, AJ, 119, 2968
Gerardy, C. L., et al. 2002, ApJ, 575, 1007
Grevesse, N., & Sauval, A. J. 1998, Space Sci. Rev., 85, 161
Heger, A., & Langer, N. 2000, ApJ, 544, 1016
Hillebrandt, W., & Meyer, F. 1989, A&A, 219, L3
Houck, J. C., & Fransson, C. 1996, ApJ, 456, 811
Jeffery, D. J., et al. 1994, ApJ, 421, L27
Kunasz, P. B., & Hummer, D. G. 1974, MNRAS, 166, 57
Lamb, S. A. 1978, ApJ, 220, 186
Lentz, E. J., et al. 2001, ApJ, 547, 406
Leonard, D. C., Filippenko, A. V., Barth, A. J., & Matheson, T. 2000, ApJ, 536, 239
Lewis, J. R., et al. 1994, MNRAS, 266, L27
Li, W.-D., Li, C., Filippenko, A. V., & Moran, E. C. 1998, IAU Circ., 6829, 1
Lucy, L. B., Danziger, I. J., Gouiffes, C., & Bouchet, P. 1991, in Supernovae, ed. S. E. Woosley (New York: Springer), 82
Lundqvist, P., & Fransson, C. 1996, ApJ, 464, 924
Marcaide, J. M., et al. 1997, ApJ, 486, L31
Matheson, T., Filippenko, A. V., Ho, L. C., Barth, A. J., & Leonard, D. C. 2000a, AJ, 120, 1499
Matheson, T., et al. 2000b, AJ, 120, 1487
Meynet, G., & Maeder, A. 2000, A&A, 361, 101
Nomoto, K., Iwamoto, K., & Suzuki, T. 1995, Phys. Rep., 256, 173
Nomoto, K., Suzuki, T., Shigeyama, T., Kumagai, S., Yamaoka, H., & Saio, H. 1993, Nature, 364, 507
Oke, J. B., et al. 1995, PASP, 107, 375
Panagia, N., et al. 1980, MNRAS, 192, 861
Patat, F., Chugai, N., & Mazzali, P. A. 1995, A&A, 299, 715
Podsiadlowski, P. 1992, PASP, 104, 717
Podsiadlowski, P., Joss, P. C., & Rappaport, S. 1990, A&A, 227, L9

Pooley, D., et al. 2002, ApJ, 572, 932
Pozzo, M., Meikle, W. P. S., Fassia, A., Geballe, T., Lundqvist, P., Chugai, N. N., & Sollerman, J. 2004, MNRAS, 352, 457
Pradhan, A. K., & Peng, J. 1995, in The Analysis of Emission Lines, ed. R. E. Williams & M. Livio (Cambridge: Cambridge Univ. Press), 8
Qiu, Y. L., Cao, L., Qiao, Q. Y., Kiss, L., Keen, R., & Hornoch, K. 1998, IAU Circ., 6841, 2
Ray, A., Singh, K. P., & Sutaria, F. K. 1993, J. Astrophys. Astron., 14, 53
Richmond, M. W., Treffers, R. R., Filippenko, A. V., Paik, A. Y., Leibundgut, B., Schulman, E., & Cox, C. V. 1994, AJ, 107, 1022
Ripero, J., et al. 1993, IAU Circ., 5731, 1
Rottenberg, J. A. 1952, MNRAS, 112, 125
Saio, H., Nomoto, K., & Kato, M. 1988, Nature, 334, 508
Schmidt, G., Weymann, R., & Foltz, C. 1989, PASP, 101, 713
Shigeyama, T., & Nomoto, K. 1990, ApJ, 360, 242
Tully, R. B. 1988, Nearby Galaxies Catalog (Cambridge: Cambridge Univ. Press)
Turatto, M., Cappellaro, E., Danziger, I. J., Benetti, S., Gouiffes, C., & Della Valle, M. 1993, MNRAS, 262, 128
Van Dyk, S. D., Weiler, K. W., Sramek, R. A., Rupen, M. P., & Panagia, N. 1994, ApJ, 432, L115
Vladilo, G., Centurion, M., de Boer, K. S., King, D. L., Lipman, K., Stegert, J. S. W., Unger, S. W., & Walton, N. A. 1994, A&A, 291, 425
Wang, L., Howell, D. A., Höflich, P., & Wheeler, J. C. 2001, ApJ, 550, 1030
Weiler, K. W., Sramek, R. A., Panagia, N., van der Hulst, J. M., & Salvati, M. 1986, ApJ, 301, 790
Wellstein, S., & Langer, N. 1999, A&A, 350, 148
Woosley, S. E., Eastman, R. G., Weaver, T. A., & Pinto, P. A. 1994, ApJ, 429, 300
Woosley, S. E., Heger, A., & Weaver, T. A. 2002, Rev. Mod. Phys., 74, 1015
Zimmermann, H.-U., et al. 1994, Nature, 367, 621